SILICON CARBIDE CAPACITIVE HIGH TEMPURATURE MEMS STRAIN TRANSDUCER

THESIS

Richard P. Weisenberger, DR01, USAF

AFIT/GE/ENG/12-43

DEPARTMENT OF THE AIR FORCE

AIR UNIVERSITY

AIR FORCE INSTITUTE OF TECHNOLOGY

Wright-Patterson Air Force Base, Ohio

AFIT/GE/ENG/12-43

SILICON CARBIDE CAPACITIVE HIGH TEMPURATURE MEMS STRAIN TRANSDUCER

THESIS

Presented to the Faculty

Department of Electrical and Computer Engineering

Graduate School of Engineering and Management

Air Force Institute of Technology

Air University

Air Education and Training Command

In Partial Fulfillment of the Requirements for the

Degree of Master of Science in Electrical Engineering

Richard P. Weisenberger, BSEE

DR01, USAF

March 2012

# SILICON CARBIDE CAPACITIVE HIGH TEMPURATURE MEMS STRAIN TRANSDUCER

Richard P. Weisenberger, BSEE

DR01, USAF

Approved:

_____   *12 Mar 12*

Ronald A. Coutu, Jr., Ph.D., P.E. (Chairman)   Date

_____   *12 Mar 12*

LaVern A. Starman, LtCol, Ph.D., USAF (Member)   Date

_____   *12 MAR 12*

Michael R. Grimaila, Ph.D. (Member)   Date

AFIT/GE/ENG/12-43

Abstract

Air Force Research Lab Air Vehicles directorate performs research on hypersonic vehicles. To verify materials or designs of hypersonic vehicles, they have a need to measure strain at temperatures exceeding 700 C. Strain sensors have the ability to measure strain. Strain is the deformation of materials due to internal stresses in a material. Internal stresses occur when a material is subjected to a force. Traditional strain sensors use Piezoresistive effects to measure strain, which is temperature dependent and making them unusable at high temperatures. This paper discusses a novel strain sensing device, sensing capacitance instead of piezoresistance. The strain sensor is modeled mathematically and simulated using Coventorware©. The results are presented here, along with recommendations for future work.

Acknowledgments

For the guidance and support of making this paper possible, I would like to thank Dr. Ron Coutu. For the support of my committee which allowed this paper to come in on time, I would like to thank Lt Colonel Lavern Starman and Dr. Michael Grimaila. For the time and support for some of the background information, Mr. Larry Kretz. Finally I would like to thank my family for their support.

Signed

Richard Weisenberger

Table of Contents

List of Figures

List of Tables

List of Symbols

A	Area
AB	Plane through a body forming a cross sectional area
ΔA	Incremental area
C	Capacitance
ΔC	Change in capacitance
C	Cubic crystalline structure
C_{DETFSS}	Capacitance in the double ended tuning fork strain sensor
$C_{Fingerset}$	Capacitance in an individual finger set
C_{Green}	Green area capacitance
C_P	Parasitic capacitance
$C_{PARALLEL}$	Parallel plate capacitance
$C_{Strainsensor}$	Capacitance in the strain sensor
C_{Yellow}	Yellow area capacitance
d	Capacitor plate distance
D	Flux density
$d\delta$	Differential elongation
dL	Differential cross sectional length
δ	Total elongation
ds	Incremental surface area
E	Modulus of Elasticity
E	Electric field
ε	Strain
ε_l	Longitudinal strain
εr	Relative permittivity to vacuum
εo	Permittivity of free space
F_o	Oscillating frequency
L	Original Length
L_s	axial strain length
L_T	length of one interdigitated finger
ΔL	Change in Length
Q	Quality factor
Q_F	Charge on a parallel plate capacitor
GF	Gage Factor
N	Line Normal to the surface
N_{AFS}	number of Axial Finger Sets
N_{IDFS}	number of interdigitated finger sets

P	Force
ΔP	Incremental force
ΔP_N	Total normal force
ΔP_S	Shear force
R	Original resistance or resistance
ΔR	Change in Resistance
ρ	Resistivity
R_G	Gage Resistance
R_S	Resistance within the double ended tuning fork system
S	Line Lies on the Surface
τ	Shearing Stress
T	Thickness of the mechanical layer
θ	Angle
σ	Normal Stress
σ_l	Longitudinal stress
V	Electric potential (voltage) applied to a parallel plate capacitor
w	Width of parallel plate capacitor
W_T	width of the interdigitated finger

List of Acronyms

AFIT	Air Force Institute of Technology
AFRL	Air Force Research Laboratory
AFRL/RB	Air Force Research Laboratory Air Vehicles Directorate
CAD	Computer Aided Design
CVD	Chemical Vapor Deposition
DETF	Double Ended Tuning Fork
LPCVD	Low Pressure Chemical Vapor Deposition
MEMS	Microelectromechanical Systems
SOI	Silicon On Insulator
PECVD	Plasma-enhanced chemical vapor deposition
SiCOI	Silicon Carbide on Insulator

SILICON CARBIDE CAPACITIVE HIGH TEMPURATURE MEMS STRAIN TRANSDUCER

I. Introduction

Air Force Research Laboratory Air Vehicles Directorate, AFRL/RB, performs research in future generation aerospace vehicles. They are at the forefront of hypersonic aerodynamic vehicles. Part of the interest in hypersonic flight is the desire to intercept missiles, deploy strike weapons that can go long ranges at high speeds, and an interest in space transport access system [21:5915-5924]. When designing hypersonic vehicles, material strength calculations require accurate material properties. This requires experimental analysis of materials based properties which use Hooke's Law of the relationship between material stress and deformation of that material [8:52]. Deformation occurs throughout the material, including at its surface. Measuring deformation at the surface is typically done using a strain sensor. AFRL/RB has the need to measure this deformation at high temperatures, often exceeding 700°C for hypersonic vehicle applications [11].

1.1 Motivation

1.1.1 Air Force Research Laboratory Organizational Requirements

Part of Air Force Research Laboratory Air Vehicles Directorate mission:

- Plans, directs, manages, and performs basic research, conducts exploratory and advanced research and development programs in air vehicle structures [20].

- Identifies and validates extreme environment, and integrated structural concepts for performance enhancements to aerospace vehicles [20].

- Development in combined environment structures technologies to improve performance of fixed-wing aerospace vehicles [20].

- Develop experimental tools for combined environment experimental verification and validation of advanced structural concepts [20].

- Provide experimental instrumentation required to support aerospace vehicle components subjected to extreme mechanical and thermal environments [20].

Part of the AFRL/RB research portfolio, is structural design and analysis of hypersonic vehicles. Hypersonic speeds refer to speeds greater than Mach 5. Hypersonic vehicles are categorized as; ballistic missiles, re-entry vehicles, space access vehicles, interceptor missiles, hypersonic cruise missiles, and single use and reusable aircraft [21:5915-5924]. Validation of aerospace vehicle components in extreme mechanical and thermal environments is required when designing hypersonic vehicles. This is achieved by determining stress in the materials when subjected to a load. This stress is measured in deformation at the surface of the materials, known as strain [14:42-89].

1.1.2 Problem Statement and Research Objectives

Measuring strain is difficult in high temperature environments, over 700°F. Current commercial strain sensors do not work within the extreme temperature environments, as explained within this paper [11]. The objective of this research is listed in the following questions:

Why do commercial strain sensors not work in high temperature environment?

How do I design a high temperature strain sensor?

How do I prove the sensor works without manufacturing it?

Within this document a high temperature strain sensor is designed, modeled and simulated using finite element simulation software. Also stress, strain, stress strain relationship is given as a background. Also discussed are measurements using traditional strain sensors, and why they do not work in extreme temperatures. An alternative design for measuring strain using a double ended tuning fork is discussed. Also discussed is manufacturing processes for making silicon MEMS devices and silicon carbide MEMS devices. Modeling and simulation of a new high temperature capacitive strain sensor made with silicon carbide is done, the device is modeled mathematically and drawn using layout software L-Edit and tested with a finite element simulator known as Coventorware$^©$.

1.1.3 Thesis Organization

The thesis is broken down into five chapters, Chapter one is the introduction, chapter 2 is background information, chapter 3 approach, chapter 4 is results, and chapter 5 is the conclusions and future work.

Chapter 1 discusses motivation in making a high temperature strain gage. It also gives the problem statement, and the thesis organization. Chapter 2 discusses the background information required in understanding stress, strain, stress strain relationship; low temperature strain measurements; the double ended tuning fork resonator; and silicon and silicon carbide manufacturing for MEMS. Chapter 3 discusses the new sensor design, fabrication, mathematical model, and Coventorware$^©$ simulations. Chapter 4 presents the results to the mathematical model and Coventorware$^©$ simulations. Chapter

5 discuses conclusions derived from the modeling and future work to realize a high temperature strain sensor.   Included in the appendix is Matlab[©] code, L-Edit©, Coventorware© processes followed by a bibliography of references.

II. Background

When a material, such as a metal, is subjected to a mechanical force, or mechanical load, stress is present. To determine stress within a material, strain in measured. Strain is the surface effect of stress within a body subjected to a force. Strain is measured using a strain sensor [14:42-89], a device which is mounted or manufactured on the straining surface that translates strain into an electrical signal. The Air Force Research Laboratory's Air Vehicles Directorate has a requirement to measure strain at high temperatures, greater than 700°F [20;11]. Most commercially available strain transducers can withstand relatively benign temperature environments or less than 700°F [7:184-197]. Higher temperature strain transducers are available, but with concerns in reliability, temperature ranges, and accuracy these developmental gages are unused [11].

Chapter II emphasizes background information in stress, strain, stress strain relationship, measurements using strain sensors, low temperature strain sensors, and the double ended tuning fork. Chapter II also discusses about silicon and silicon carbide as a material for using in MEMS. It also discusses manufacturing techniques of silicon and silicon carbide MEMS.

2.1 Stress and Strain

Stress is the measure of forces internal to a body and strain is the measure of deformation of the displacement between particles [15:3-41]. Stress and strain are related through material properties, known as Young' Modulus. This section discusses stress, strain, and the stress-strain relationship.

2.1.1 Stress

When a body is acted on by either internal or external force, or system of forces, it is subjected to stress. It is generally thought of as the forces are transmitted from one particle to another [14:42-89]. These forces get distributed either on the surface or internally through the body. Stress is the way the forces magnitude is distributed within a material. The materials ability to withstand the forces is known as its resistance to stress. Also, stress can be thought of as the effect of forces on part or the entire surface of a body [14:42-89]. For the purpose of this paper stress will be understood as force per unit area.

Figure 1 a) shows a body acted upon by multiple forces, P1, P2, P3, and P4. A plain through the body is depicted as AB, Figure 1 b). One element of these forces is represented by an incremental force, ΔP, acting on an incremental area, ΔA. We can now define stress at a single point, equation (1).
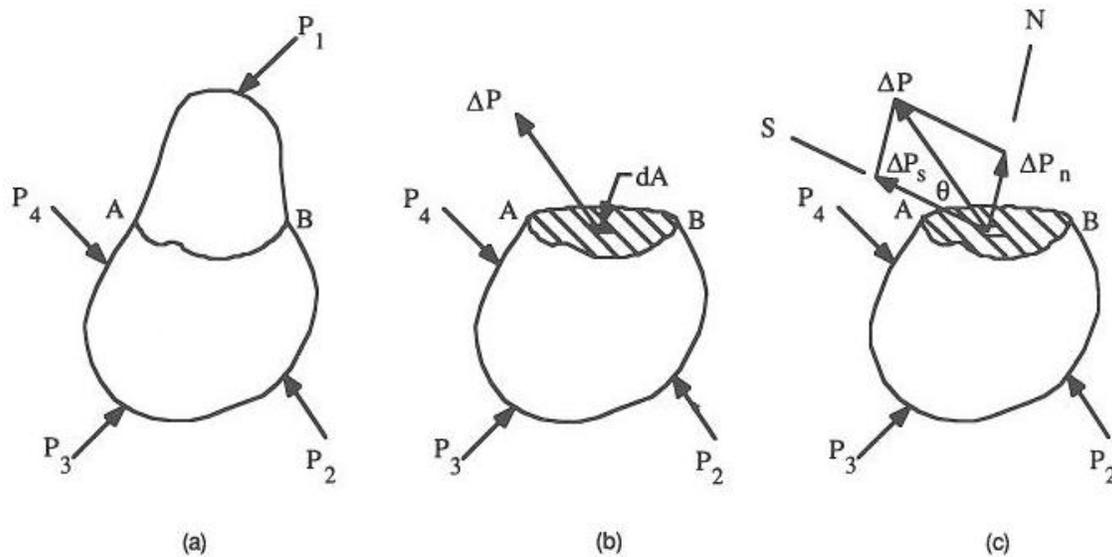
Figure 1 A body with external forces. (Reproduced without permission from [14:14].).

a) a body acted upon by multiple forces, b) one element force per element area, c) normal and

shear forces.

$$Stress = \lim_{\Delta A \to 0} \left[\frac{\Delta P}{\Delta A}\right] \tag{1}$$

ΔP at angle θ from the surface as shown in Figure 1 c), which is not necessarily normal to the surface, Line N, which is normal to surface, and Line S, lies on the surface, from Figure 1 c), breaks ΔP into ΔP_N, total normal force, and ΔP_S, total shear force. Stress can now be broken down into normal stress (σ), in the normal direction N, and shear stress (τ), along surface N. Normal stress will be in tension, or tensile stress, increasing (positive) stress, if the material separates on opposing sides of the section. Normal stress will be in compression, compressive stress, or decreasing (negative) stress, if the material tends to push together on opposing sides. Shear stress has the material on one side of the section to move by the material on the other side of the section [14:42-89].

Uniformly distributed stress occurs when each force acting on an area gets distributed uniformly over the area. Each element of the area is subjected to an equal loading value. Stress at each element will be at the same magnitude which is defined as the average stress value [14:42-89]. This is determined by dividing the total force by the total area. Uniformly distributed stress is defined by equation (2). The assumption is that stress is uniformly distributed within a body.

$$Stress\ (average) = \frac{Total\ Force}{Entire\ Area} = \frac{P}{A} \tag{2}$$

2.1.2 Strain

Where stress exists in a material there is some type of deformation of that material. This is known as strain and represented by ε [14:42-89]. Like stress, there are two types of strain, linear strain and shear strain [14:42-89]. Linear strain can obtain two notable states, in tension or compression [14:42-89]. Linear strain will be in tension, tensile

strain, or increasing (positive) strain, if the material lengthens in a straight line [14:42-89]. Linear strain will be in compression, compressive strain, or decreasing (negative) strain, if the material shortens in a straight line [14:42-89].

If a bar of some length L is loaded longitudinally. Assume the bar elongates uniformly, and the cross sectional area is originally shaped as a plane and perpendicular to the loading axis and remains so throughout the elongation process. This bar is represented in Figure 2. Unit strain of elongated bar is given by equation (3), which represents average strain. L is the original length of the bar, and δ is the total elongation of the bar [14:42-89].

$$Strain = \varepsilon = \frac{\delta}{L} \tag{3}$$
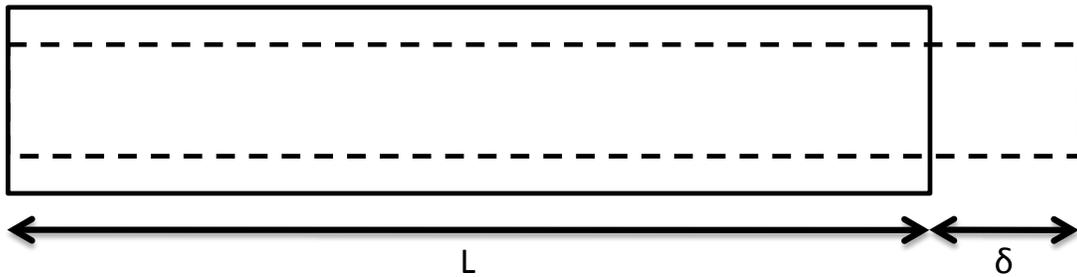
Figure 2 Bar subjected to Elongation

Since strain in equation (3) is average strain, and the bar represented in Figure 2 assumes a constant cross section bar, equation (3) cannot be used if the bar's cross sectional area is not constant or of the load is not uniformly distributed. Then strain per unit determined by differential elongation or *dδ* of a cross sectional length *dL*. Unit strain at a point on the bar in Figure 2 is expressed as equation (4) [14:42-89].

$$\varepsilon = \frac{d\delta}{dL} \tag{4}$$

2.1.3 Stress and Strain

Stress and strain are depended upon each other, and related through material properties. Robert Hooke stated this relationship is accomplished by a constant of proportionality known as the modulus of elasticity, E [14:42-89]. For the bar subjected to elongation is shown as equation (5). The variable σ_l is known as the longitudinal stress, elongation direction. The variable ε_l is known as the longitudinal strain.

$$\sigma_l = E\varepsilon_l \tag{5}$$

2.2 Strain Measurements

When materials are mechanically validated, a force is introduced into it and the resultant stress in the material can be measured and reveals important characteristics, such as Young's Modulus, about the material. Measuring stress directly is not easily done. However stress can be determined by measuring strain on the surface and through material properties stress is derived, using equation (5). Strain measurements are performed by devices called strain transducers, or more commonly strain gages. This section goes over the strain measurement, foil strain gages, and high temperature strain measurements.

2.2.1 Strain Measurements

Let's assume a conductor is unrestrained laterally and is strained in its axial direction, its length will change and its cross section will also change, this effect is known as the Poisson Effect [14:42-89], this is shown in Figure 3. If the strain increases the length of the conductor its cross sectional area will decrease, and vice versa if strain decreases the length its cross sectional area will increase. Also resistivity of the conductor material will change because of the arrangement of the atoms inside, but the

volume does not change. Resistivity, equation (6), shows that these three elements, change in length (L), cross sectional area (A), and resistivity (ρ), will change the overall resistance (R) in the conductor [15:3-41].

$$R = \rho \frac{L}{A} \qquad (6)$$
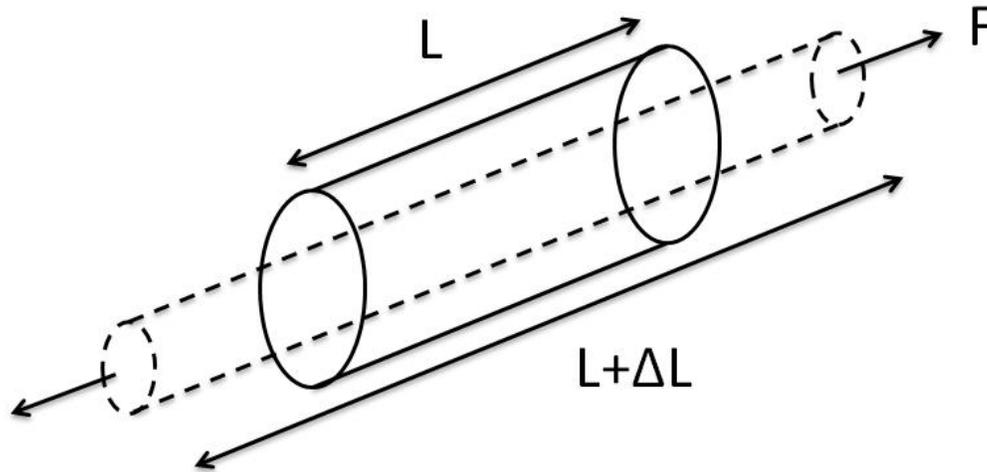
Figure 3 Strained Conductor (Shown in Tension)

2.2.2 Foil Strain Gages

The more conventional strain transducer, known as a strain gage, uses an insulating flexible backing that supports a metallic foil element. The flexible backing is adhered to the straining surface, such as a metallic beam put under stress. The object becomes deformed when the backing flexes and the foil becomes deformed, and changes its electrical resistance. This change in resistance is measured and strain can be calculated using the gage's gauge factor, GF. Equation (7) depicts the relationship of resistance to strain and gage factor. Where ΔR = Change in resistance due to strain, R_G = undeformed resistance, GF = gauge factor defined by the manufacturer, and ε is strain. Which strain

is simply defined, in equation (8), as a change in bar length (Δl) over the original length

(L)

$$GF = \frac{\left(\Delta R / R_G\right)}{\varepsilon} \tag{7}$$

$$\varepsilon = \frac{\Delta l}{L} \tag{8}$$

Figure 4 depicts an example of the strain gage in various states. Figure 4 a) is unstrained state, which depicts the foil as a "strain sensitive pattern". The white box in the figure is the device's flexible backing, and the gray is the strained surface. Figure 4 b) depicts the object strained in tension or increase in resistance (ΔR) thus greater strain. Figure 4 c) depicts the object strained in compression or a decrease resistance (ΔR) thus less strain.
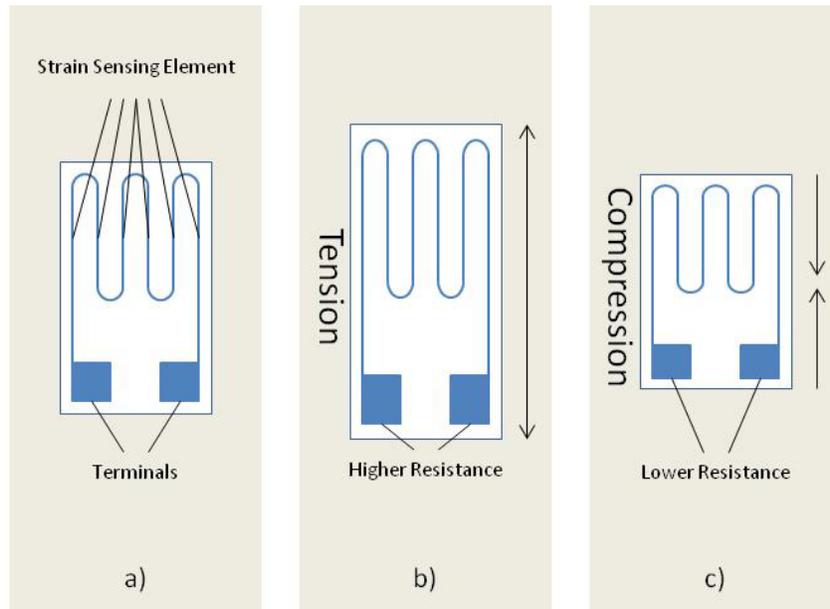
Figure 4 Strain gage in 3 states, a) depicts the unstrained state, b) depicts strain in the tension state, and c) depicts strain in the compression state

2.2.3 High Temperature Strain Measurements

The insulating flexible backing typically cannot withstand the extreme environments. This makes these types of sensors not usable in high temperatures. If a flexible backing is invented which can be used in extreme temperatures, there is still an issue with the metallic foil's resistivity changing as a function of temperature. Thus, strain gages that utilize piezoresistive elements undesirable at high temperature [8:52].

2.2.4 Applications of Strain Sensors

There are different applications of strain sensors. One application of strain sensors is the investigation of tension or compression strain caused by tension or compression mechanical forces, known as mechanical loads. Compression occurs when a material is loaded from one end toward the material. Tension occurs when a material is loaded from one end away from the material. Figure 5 a) depicts an unloaded bar. Figure 5 b) depicts a bar loaded in compression. Figure 5c depicts a bar loaded in tension [8:52]. Strain sensors are used to how well materials deal with these loads in compression and tension.
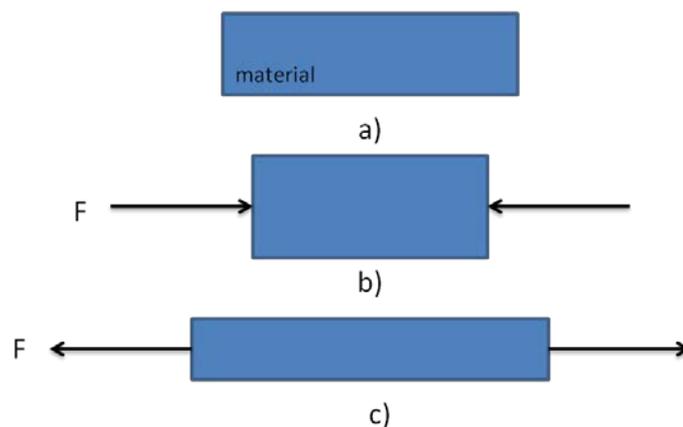
Figure 5 Material Subjected to Loads. a) Unloaded, b) Compression Loaded, c) Tension Loaded

Another application of strain sensors is the measurement of bending moments. A bending moment occurs when load is applied transaxially on something like a beam, where strain on top of the beam is greater than strain on the bottom of the beam, and vice versa [8:52]. Figure 6 depicts a bar subjected to a moment arm.
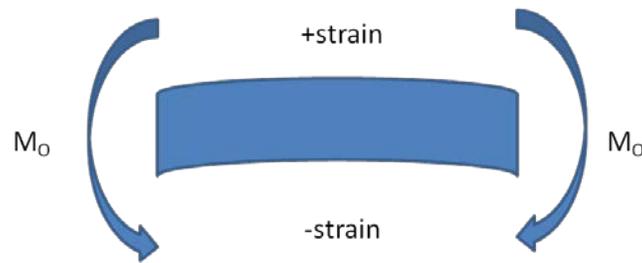
Figure 6 Bar Subjected to a Moment Arm

Many variations of tension, compression, and moment arm loading exist providing endless possibilities of configurations. Strain sensors can be made into force sensors, using these configurations [1]. Sensors can be made into health monitoring devices for load reaction structures and equipment put under load.

High temperature strain sensors have these same applications although at temperatures exceeding 700°C. High temperature environments requiring strain sensing include oil and gas equipment, nuclear and power station equipment [6], and aerospace hypersonic vehicles [21:5915-5924].

Hypersonic vehicles experience temperatures in excess of 500°C on inlet ramp surfaces at Mach 5 [21:5915-5924]. On that same surface, temperatures exceed 700°C at Mach 6. Another point on the hypersonic engine is the stagnation wall of leading edge, which experiences 700°C at Mach 5 [21:5915-5924]. Many points on the hypersonic vehicle could use a high temperate strain sensor to measure the effects of load introduced to them. During the design and verification process, conditions must be duplicated at

which the intended material would be subjected to in actual flight conditions. Depicting the reason why a high temperature strain sensor is required for hypersonic vehicles and why AFRL/RB needs them.

2.3 The Double Ended Tuning Fork

To alleviate high temperature effects on strain measurements an alternate approach could be taken. Double Ended Tuning Fork resonant sensors are already in use for high precision strain measurements [22:841-845]. This MEMS device can be made from Silicon Carbide for high temperature strain sensor applications like the one shown in reference [1] which was found to work at temperatures around 300°C with resolution found to be 0.11 micrometers. The double ended tuning fork could also be made from silicon and coated in silicon carbide to bring the operating temperature up to 500°C with resolution of 0.2 micrometers at 10kz to 20kz as shown in reference [2:643-646]. This section discusses the double ended tuning fork's operation, strain sensing using the double ended tuning fork.

2.3.1 Concept of operation

The double ended tuning fork is modeled as a spring mass damping resonator system. The concept is drawn in Figure 7. A shuttle mass is suspended over a substrate, and is attached at each end to anchors. The anchors are attached to the substrate. Attached to the shuttle mass are interdigitated fingers. Built next to the interdigitated fingers are other interlaced interdigitated fingers which are attached to the substrate via anchors [22:841-845]. The shuttle mass is allowed to move toward, and subsequently away from, the interlaced interdigitated fingers [22:841-845].
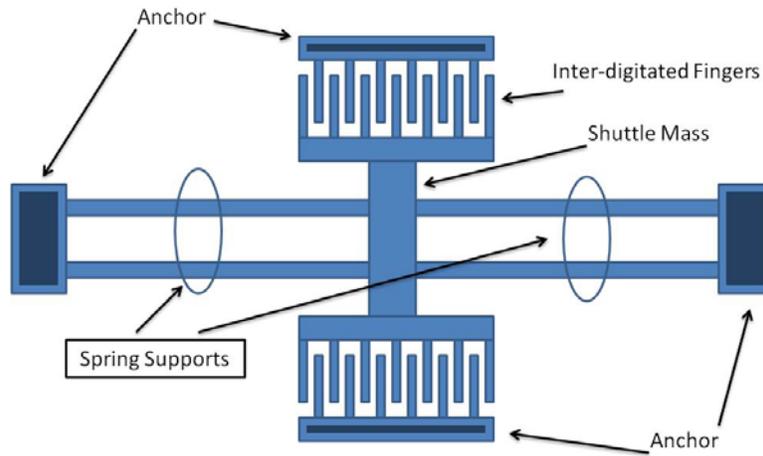
Figure 7 The Double Ended Tuning Fork (DETF)

2.3.2 Sensing Strain Using the Double Ended Tuning Fork (DETF)

To make a double ended tuning fork strain sensor, the same techniques are used for making a traditional double ended tuning fork resonator. A double ended tuning fork is produced on top of a flexible backing of a minimum thickness, so strain is transmitted through to the sensor. Figure 8 depicts such a sensor.
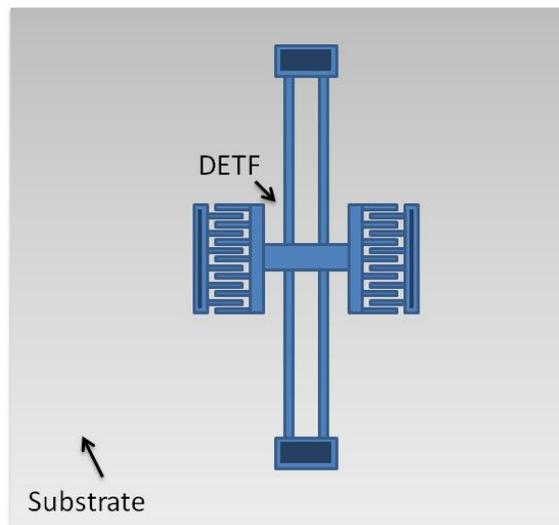
Figure 8 Double Ended Tuning Fork (DETF) Strain Sensor with Flexible Backing Substrate

The double ended tuning fork construction is summarized in Figure 7. The double ended tuning fork strain sensor works when stress occurs from the sensed surface to the surface of the substrate, directly below the double ended tuning fork MEMS structure. When it is strained the distance between the interdigitated fingers anchor and the spring support anchor gets larger, as shown in Figure 9. The anchors are mechanically attached to the substrate. The entire body of the movable double ended tuning fork, shuttle mass, spring supports, interdigitated fingers, and anchor are all a part of the shuttle assembly. The anchor and interdigitated fingers on each side of the shuttle mass are to separate fixed components. The shuttle mass assembly can move axially, to and away from the interdigitated anchor fingers.
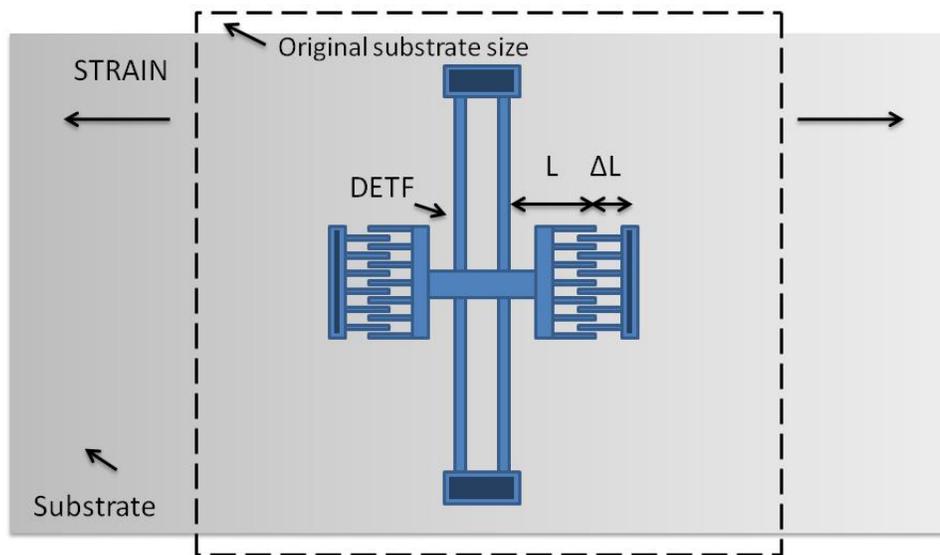
Figure 9 Strained Double Ended Tuning Fork

Figure 8 is the device in an unstrained state. Figure 9 shows an axially strained in the positive direction, or positive strain, +ε. Conversely Figure 10 shows a double ended tuning fork strain sensor in compression, or negative strain, -ε.
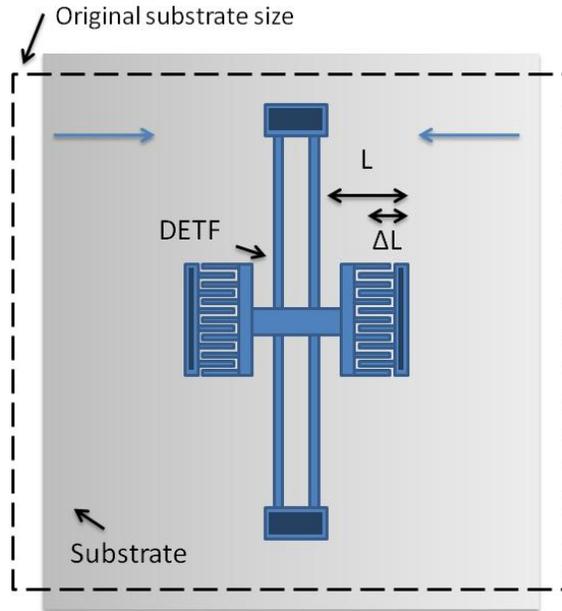
Figure 10 Axially Strained Double Ended Tuning Fork in Compression

Strain is the change in length, ΔL, over the original length, L, equation (9), the device measures strain by the change in distance between the anchors changes the gap between the shuttle's interdigitated fingers and the anchors interdigitated fingers. The interdigitated finger set can be modeled as a parallel plate capacitor. Figure 11 shows the unstrained interdigitated finger parallel plate capacitor. Figure 12 shows the strained interdigitated finger parallel plate capacitor. This is discussed later.

$$Strain = \varepsilon = \frac{\Delta L}{L} \tag{9}$$
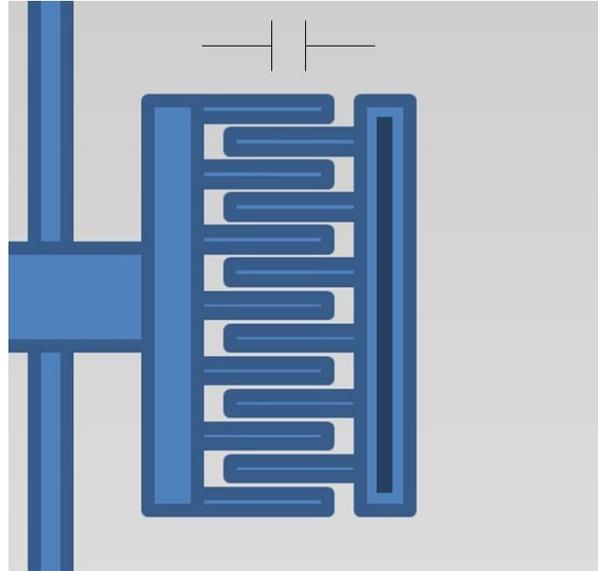
Figure 11 Unstrained Interdigitated Capacitive Fingers
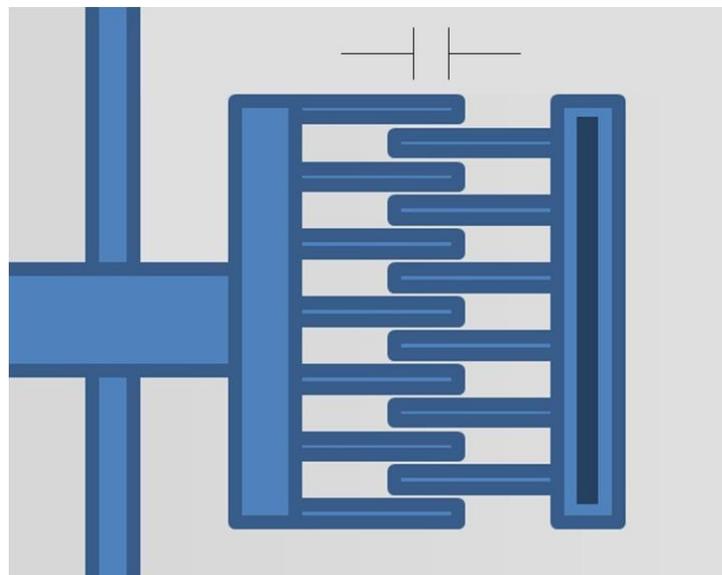
Figure 12 Strained Interdigitated Capacitors Fingers

2.3.3 Oscillation of Double Ended Tuning Fork Strain Sensor

The sensor is driven by a frequency at which the shuttle mass oscillates. That frequency is dependent on capacitance. When strain is applied to the substrate, the

interdigitated fingers separate and the oscillation frequency changes [22:841-845]. The frequency is adjusted again until oscillation is again achieved.

Capacitance in the double ended tuning fork strain sensor can be measured using equation (10). C_{DETFSS} is capacitance in the double ended tuning fork. Frequency output is f_0, and resistance of the double ended tuning fork system is R_S [22:841-845].

$$\frac{Q}{2} C_{DETFSS} = \frac{1}{4\pi f_o R_S} \qquad (10)$$

R_S is the impedance of the measurement hardware. The variable f_o is the oscillation frequency. As reported in [22:841-845] there is a risk of loss in detection of capacitance in the double ended tuning fork strain sensor, C_{DETFSS}, due to parasitic capacitance, C_P, in the connection to the sensing system. C_{DETFSS} could be much smaller than the parasitic capacitance, causing the loss in detection. Reduction in this parasitic capacitance could be difficult [22:841-845].

2.4 Capacitance

When a potential is applied between two conductors electric field is created. When the two conductors are separated and an electric field is produced between them a capacitance is present. This section goes over how capacitance is formed between two conductors separated by a distance which has a potential between them.

2.4.1 Capacitance and Electrostatic Field

As stated, the double ended tuning fork's interdigitated fingers can be modeled as a parallel plate capacitor. The parallel plate capacitor has a mathematical model of equation (11), and shown in Figure 13. In the model $C_{PARALLEL}$ is parallel plate capacitance; A is the plate's area, length, L, multiplied by width, w. The distance

between the plates is shown as d, also ε, ε_r and ε_0 are permittivity, relative permittivity or permittivity relative to vacuum, and permittivity of free space, or vacuum permittivity, respectively. Permittivity is the ability a material has to store energy when voltage applied across the material. A parallel plate capacitor is shown in Figure 13. Relative permittivity for our device will be that of open air, or $\varepsilon_r = 1.0$.

$$C_{PARALEL} = \frac{\varepsilon A}{d} = \frac{\varepsilon_r \varepsilon_o LW}{d} \tag{11}$$
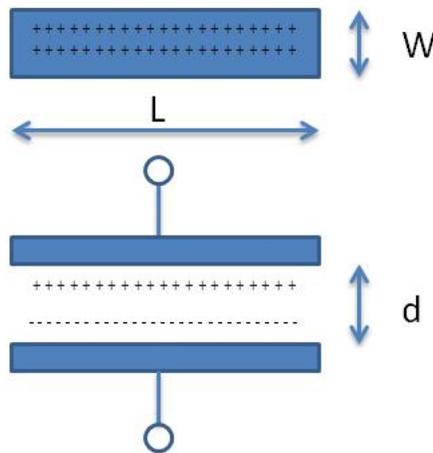
Figure 13 Parallel Plate Capacitor Simple Model

Consider the parallel plates in Figure 13 made of perfectly conducting plates. When a potential, V, is applied across the plates, an electric field, E, is created [16:127-134]. The potential lines occur from the high plate potential to the low plate potential, shown in Figure 14 [16:127-134]. The equation for parallel plate capacitance, equation (11), can be rewritten with respect to charge Q_F, Equation (12). The relationship of charge, Q_F, to surface, S, and electric flux density, D, is derived from Guass Law and written in equation (13). Voltage from the source is obtained by integrating the electric field, E, between two points, P_1 and P_2, on the surface of the conductors and is depicted in equation (14).

$$C = \frac{Q_F}{V} \tag{12}$$

$$Q_F = \oint_S D \circ ds \tag{13}$$

$$V = -\int_{P_1}^{P_2} E \circ dl \tag{14}$$
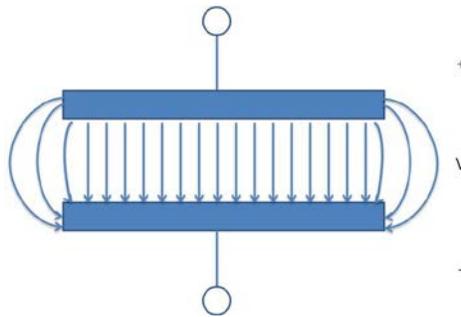
Figure 14 Electric Field Lines for a Parallel Plate Capacitor

If we combine equations (12), (13), and (14), and substituting flux density with the relationship D=εE, we get equation (15) [16:127-134]. This shows that capacitance is dependent on electric fields and geometry [16:127-134].

$$C = \frac{\oint_S D \circ ds}{-\int_{P_1}^{P_2} E \circ dl} = -\varepsilon \frac{\oint_S E \circ ds}{-\int_{P_1}^{P_2} E \circ dl} \tag{15}$$

In the thesis found in reference [18:12,14,26], he modeled the double ended tuning fork in a three dimensional finite element from the top down. The tool depicted the electric field lines as shown in Figure 15 [18:12,14,26]. Figure 16 depicts the electric field lines, solid lines, from the end view [18:12,14,26]. The dashed lines are electric potential gradient lines. There were no mathematical functions for these field lines presenting in reference [18:12,14,26].
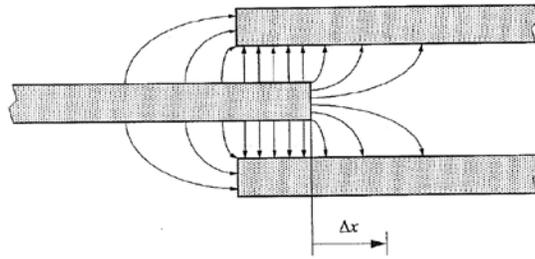
Figure 15 Top Down View of Interdigitated Fingers Electric Field Lines (Reproduced from Reference [18:12,14,26] without permission)
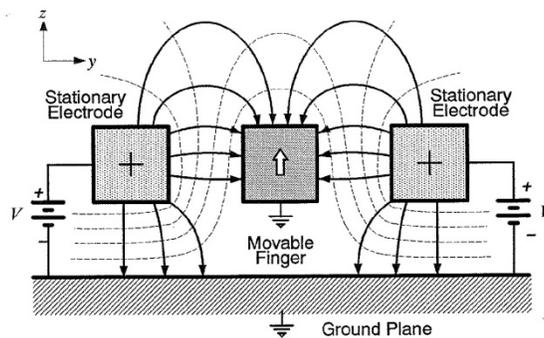
Figure 16 End View of Interdigitated Fingers Electric Field Lines (Reproduced from Reference [18:12,14,26] without permission)

2.5 Silicon as a Mechanical Structure

Silicon is the most dominant material used MEMS devices today. This section goes through the material properties of silicon as used in MEMS devices.

2.5.1 Material Properties

Silicon is a dominate element used in the manufacturing of MEMS devices. Here are a few of these reasons. First, silicon is a cheap and well characterized material which is readily available, which comes from the integrated circuit industry's years of development and research. Second, a large number and variety of processing techniques and processes matured and are available to manufacture devices with little to no

adaptation for MEMS. Third, the possibility of integrating devices with control and signal processing integrated circuits, additionally the mechanical, electrical, and physical properties is has give it an advantage in MEMS devices [15:3-41].

Silicon has other advantages. Thermal oxides can be grown or deposited easily and at relatively low temperatures, between 200 and 1150°C [23:2-9], and growth rates are dependent on temperature. Thermal oxides give the added advantage of a sacrificial layer that can be removed, or dissolved, with hydrofluoric acid (HF). HF is highly selective between Si and SiO_2. Mechanical layers are made from Si within SiO_2, SiO_2 is dissolved and a clean mechanical layer remains with unaltered properties.

One of the advantages silicon has in producing MEMS devices is the opportunity to use dopants to change some properties of silicon allowing for more flexibility in manufacturing and operation. For instance if silicon is doped with group three elements, which is missing the fourth electron in the valance band creating a hole, this causes the resistivity to decrease. Subsequently if silicon is doped with group five elements, extra electron in the valance band or donor electron allowing a free electron in the doped material, the material becomes more electrically conductive. These properties can be exploited to change how the device responds to signals applied to it.

Silicon can be broken down by two types, Single-Crystalline Silicon and Polysilicon [23:2-9]. Silicon has a diamond structure, which is a relatively brittle material to work with. Single-Crystalline silicon, or crystalline silicon, can be grown and subsequently made into pure crystalline wafers with low defects. These wafers can easily have large surface areas, larger than 8 inches in this manner [23:2-9]. Crystalline silicon serves key functions in MEMS processes. It is the most versatile material for bulk

23

micromachining, well characterized etchants and masking materials are available. It is used as a mechanical platform, on which devices are surface micromachined, or grown on the surface and shaped into devices using many techniques. Crystalline silicon is the primary material integrated circuits are manufactured on. Some selected properties of crystalline silicon are shown in Table 1.

Table 1 Selected Properties of Crystalline Silicon from [23:2-9]

Property (unit)	Unit	Value
Yield Strength	(10^9 Nm^{-2})	7
Knoop Hardness	kgmm^{-2}	850
Young's Modulus (100) Orientation	GPA	160
Poisson's Ratio (100) Orientation	gcm^{-3}	0.28
Density	cm^{-3}	2.33
Lattice Constant	Å	5.435
Thermal Expansion Coefficient	10^{-6}K^{-1}	2.6
Thermal Conductivity	Wm^{-1}K^{-1}	157
Specific Heat	Jg^{-1}K^{-1}	0.7
Melting Point	°C	1410
Energy Gap	eV	1.12
Dielectric Constant		11.9
Dielectric Strength	10^7V^{-1}s^{-1}	3
Electron Mobility	cm^{2}V^{-1}s^{-1}	1450
Hole Mobility	cm^{2}V^{-1}s^{-1}	505

Polysilicon, Poly-Si, is combined with silicon dioxide, SiO_2, and silicon nitride, Si_3N_4 to form a powerhouse of fabrication possibilities. Poly-Si is the most commonly used material for surface micromachined MEMS, and is used as the primary structural material [23:2-9]. Si_3N_4 is used for electrical isolation with crystalline silicon wafer. Many processes are commercially available.

2.6 Silicon Carbide as a Mechanical Structure

Silicon Carbide, SiC, is material that has possibilities to be used in harsh environments, which includes temperature, chemical resistance, and radiological resistance to name a few [13:1594-1609]. This section goes through the material properties of silicon carbide as used in MEMS devices.

2.6.1 Material Properties

SiC is a one-dimensional polymorphism called polytypism and exists in more than 250 structural polytypes [4:5-12]. There are only three crystalline structures; cubic, hexagonal, and rhombohedral. All of the polytypes have identical planar arrangement of silicon and carbon atoms. The differences in the polytypes are in the way the planar arrangements are stacked. The order of stacking determines the types of close packed structures and their properties. When the layers are stacked a certain way they are depicted with the conventional nomenclature with a number of SiC double layers with the appending letter, C for cubic, H for hexagonal, R, for rhombohedral. For example 3C-SiC has cubic lattice with three layers. Each polytype exhibits different properties, for example 3C-SiC, three cubic layers of SiC, has a bandgap of 2.2eV and 4H-SiC, four hexagonal layers, has a bandgap of 3.4eV [4:5-12]. A summary of selected polytypes is given in Table 2.

Table 2 Material Properties of 3C-SiC and 6H-SiC from source [4:5-12] Young's Modulus from source [13:1594-1609].

Property (unit)	Unit	3C-SiC	6H-SiC
Yield Strength	$(10^9\ Nm^{-2})$		
Knoop Hardness	kgmm-2	3300	2917
Young's Modulus	Gpa	448	448
Density	gcm-3	3.21	3.21
Lattice Constant	Å	4.359	a0: 3.08 c0: 15.12
Thermal Expansion Coefficient	$10^{-6}K^{-1}$	2.9	4.2
Thermal Conductivity	$Wcm^{-1}K^{-1}$	4.9	4.9
Sublimes at	°C	T>3100	T>3100
Energy Gap	eV	2.2	2.99
Dielectric Constant		9.7	10
Electron Mobility	$cm^2V^{-1}s^{-1}$	1000	400
Hole Mobility	$cm^2V^{-1}s^{-1}$	40	50

2.7 Silicon Carbide Manufacturing Techniques

Silicon Carbide, SiC, is more difficult to fabricate with [13:1594-1609]. This section goes fabrication processes of silicon carbide when fabricating MEMS devices.

2.7.1 Bulk Micromachining

Bulk micromachining is the selective removal of regions of material from its substrate as shown in Figure 17 and Figure 18. Simple regions can be etched away or the entire wafer can be dissolved away. Bulk micromachining is useful for relativity large sculpturing of the surface or backside of wafers.

There are two types of wet bulk etching, isotropic and anisotropic. Isotropic etching dissolves or etches in all directions of a material, shown in Figure 17. It will also undercut or etch below the mask area. Agitation causes more rounded features. Anisotropic etches only along a crystalline plane at well defined angles shown in Figure

18.   For example, the etching solution for an anisotropic etch is potassium hydroxide (KOH) water and alcohol, which etches the <100> and <110> planes of silicon at high a much higher rate than the <111> plane, <100>, <110>, & <111>. An important thing to know is that plane <100> intersects plane <111> at an angle of 54.74 degrees, as shown in Figure 18 [10:129-138]. Dry etching is similar to wet etching but uses plasma instead of a liquid etchant. Conventional bulk micromachining designed for silicon can also be used on silicon carbide, single crystalline, poly, and amorphous. A process of bulk micromachining 3C-SiC used inductively coupled plasma etch using SF_6 and O_2 gas mixture. This plasma etch process etched isotropically [4:5-12]. Another etch process, as described in [1], using HBr and Cl_2 in a dual plasma source etch chamber which produces high density plasmas.
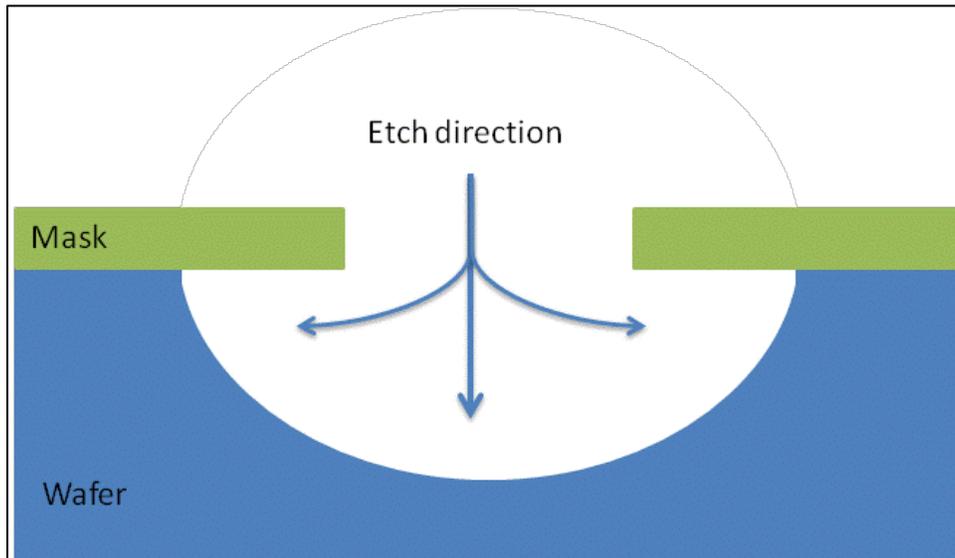
Figure 17 Bulk Micromachining Using Isotropic Wet Etch
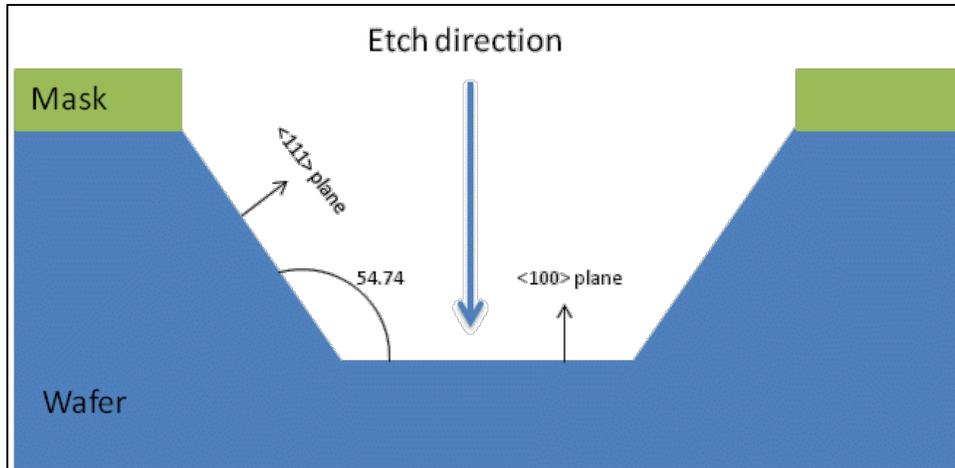
Figure 18 Bulk Micromachining Using Anisotropic Wet Etch

2.7.2 Surface Micromachining

Surface micromachining builds up structures on the surface of parent wafers by using lithography processes, deposition, and shaping the deposited materials. Commonly using silicon, silicon dioxide, polysilicon, or phosphosilicate glass (PSG, is grown or deposited on a silicon parent wafer, it is patterned using a mask layer such as a polyimide and wet or dry etched [10:271-273].

Polycrystalline silicon Carbide, Poly-SiC, is an attractive mechanical layer that can be deposited onto suitable sacrificial layers, such as SiO_2. Poly-SiC can be deposited using plasma-enhanced chemical vapor deposition, (PE) CVD. Depending on the temperature, ranging from 200 to 1000°C, the deposited SiC could be amorphous, low temperature, or polycrystalline, high temperature.   Poly-SiC can be used as a mechanical layer to perform a mechanical task [13:1594-1609]. Figure 19 shows a Poly-SiC mechanical layer, in the form of a cantilever, possibility grown using PECVD.
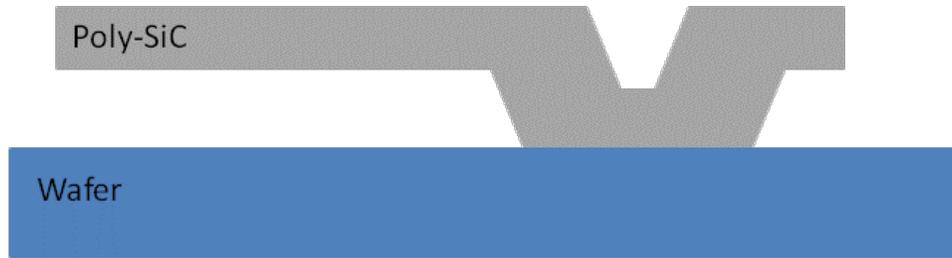
Figure 19 Poly-SiC Cantilever on a sutible substrate

Oxidation is the process of adding oxygen to Si or SiC to grow an oxide layer. The oxide layer can be used as a sacrificial layer to construct a mechanical device, such as the cantilever in Figure 19, or a dielectric in an electrical device. A thick layer, greater than 1µm, of oxide can be grown on silicon by exposing it to oxygen at temperatures greater than 1000°C. Hydrogen is added to enhance the oxidation rate. The process for silicon occurs when silicon is subjected to high temperatures, above 1000°C [13:1594-1609], and the oxide is grown when Si reacts with O_2 to form SiO_2 and CO. The process is similar to Si with SiC, SiC reacts with O_2 to form SiO_2 and CO, but the oxide grown on SiC is slower because SiC is less likely to dissociate and react with oxygen, than something like silicon. To form the same 1µm oxide is much longer for SiC than Si. Larger oxide layers, such as 3µm or larger, could take subsequent oxide growth processes [13:1594-1609].

Metals on devices are used as metal contacts, ohmic contacts, and Schottky contacts, all useful in MEMS and Microelectronics. High temperature metals with high melting points such as Nickel (Ni) or Tungsten (W) deposited on SiC, are generally used on devices intended for high temperature applications. Although the best and most widely used ohmic contact on SiC is Aluminum (Al). Aluminum is easily deposited using traditional Si processes, sputtering or evaporation. Al melts at 600°C, so for high

29

temperature applications, greater than 700°C, Al is not suitable. Other metals such as Ni,

W, and Mo make ohmic contacts on 3C-SiC [13:1594-1609]. Sputtering occurs when

energetic ions are bombarded with a target made of the required deposited material.

Atoms at the surface are knocked loose and transported to the surface. Evaporation

occurs when metals are heated until the point of vaporization. Evaporated metals form a

thin film covering the entire wafer [10:279].

To fabricate MEMS devices using SiC, selective etching is required to pattern the

SiC films. Traditional Si devices are patterned by dry plasma or wet chemical etching.

To wet etch poly silicon carbide thin films utilizes submersing the wafer in a chemical

bath of a fluorinated compound, Such as CF_3, CHF_3, NF_3, or SF_6 [10; 271-273;13:1594-

1609]. A wet etch process can also remove oxide, such as HF [10; 271-273;13:1594-

1609]. Dry etching utilizes a plasma to remove atoms from the thin film, such as a RIE.

Plasma is created by applying a radio frequency electromagnetic field to the wafer. The

oscillating electric field ionizes the O_2 molecules by stripping electrons [10:271-279;11].

Doping is the process of creating a positively or negatively charged material to

create a PN junction or transistor. Ion implantation deposits dopants by directly

bombarding the Poly-SiC or Poly-Si with high energy ions of the dopant. Ion

implantation has destructive effects. Usually following the ion implantation is an

annealing step, high temperature treatment, which repairs the damaged lattice and

activates the dopants. In-Situ doping is performed by the introduction of the dopants to

the Poly-SiC or Poly-Si at the same time polycrystalline layer is deposited, usually by a

chemical vapor deposition process (CVD). SiC is chemically inert, only ion implantation

and *in situ* doping is possible. In-situ doping is preferred due to the simplified process,

compared to ion implantation, and excessive damage of the material is minimized and is

easily incorporated into LPCVD processes.

III. Methodology

An examination of the resonant strain sensor yields some problems, mostly the dependence on tuning to the resonant frequency to determine the strain. Also conventional piezoresizitive sensor is dependent on temperature dependent resistance. To fulfill the requirement of the design of a high temperature strain sensor this chapter describes a new sensor designed to work the high temperature environment. To fulfill the requirement to prove the sensor works without manufacturing it, mathematical equations are derived and are plotted, also layout drawings are developed, which are simulated using Coventorware[©].

3.1 Silicon Carbide Process

As stated silicon carbide is a material that is more impervious to high temperatures. At the time of this paper there is no commercially available silicon carbide process, which makes developing one important. This section discusses the general process to manufacture silicon carbide MEMS devices, of which are used in the Coventorware© simulations. It is a simplified process, details to the process including the process followers are not included, because no sensor is to be manufactured in this research endeavor.

The overall process of making the sensor begins with a handle silicon wafer. An oxide is grown, with a poly-SiC "flexible backing" layer grown on top. This makes a SiCOI or silicon carbide on insulator wafer. A nitride passivation layer is added for signal isolation. N-type doped poly-SiC traces are formed, for signal egress. A second sacrificial oxide layer is grown within the poly-SiC, and it is patterned to form the anchors. The poly-SiC mechanical layer is added and patterned to form the interdigitated

finger. After the device is created, the mechanical layer is released along with the sacrificial oxide between the carrier wafer and the "flexible backing" poly-SiC, and is complete. The completed process is depicted as a side profile in Figure 20. This process is explained in greater detail below.

Figure 20 Silicon Carbide Process to Make the Strain Sensor

3.1.1 Silicon Carrier Wafer

An off the shelf wafer is selected as a carrier wafer. The carrier wafer allows a stable surface to build upon in subsequent manufacturing techniques. The size chosen is a 3-inch, 330mm, in diameter off the shelf wafer from Silicon Inc. [17].

3.1.2 First Sacrificial Oxide Growth onto Wafer

The first sacrificial oxide layer is added, the layer is called SAC1. This layer is added to allow a way to remove the sensor from the carrier wafer when processing is done. Thermal oxide is grown over the entire wafer to 2µm using a wet thermal oxide process [9:43-44].

3.1.3 Poly-SiC Sensor device Substrate formation

A poly silicon carbide sensor device substrate layer is deposited onto the sacrificial oxide layer. Nitrogen doped Poly-SiC film is deposited by Low Pressure Chemical

Vapor Deposition reactor, LPCVD. The LPCVD reactor deposits Poly-SiC at 900°C using SiH_2Cl_2, 100% solution, and C_2H_2, 5% solution with H_2 gas. SiH_2Cl_2 provides the silicon, C_2H_2 provides the carbon, and the dopant is provided by NH_3. This process is sourced from [1]. The poly-SiC layer is grown to 16µm.

3.1.4 Passivation Layer Formation

To isolate the signal lines from the device substrate, a silicon nitride layer is deposited. Silicon nitride is deposited onto the poly-SiC substrate layer using a LPCVD process described in [12;89,160-162] at 750°C to a thickness of 0.2µm. The device's substrate is patterned using photoresist, which the sensor's pattern substrate and poured onto the edge of the oxide around the parameter, and submerge the wafer in Buffered Hydrofluoric Acid, which etches 0.5 nanometers a minute [12;89,160-162].

3.1.5 Device Substrate Patterning

The substrate pattern is etched into the poly-SiC layer using a dual plasma source etch chamber, capable of high density plasmas, similar to the one in [1]. The etchant is a vapor mixture of HBr and Cl_2. According to [1] the etch rate for this process is 2500 angstroms per min, giving us an hour and 4 minutes. The selectivity of SiC to SiO_2 is 5:1 according to [1].

3.1.6 Signal Line Layer Formation and Patterning

Signal egress from the mechanical layers to the signal pads is done using another nitrogen doped poly-SiC layer. This layer is deposited, using the previous technique described in section 3.1.3, to a thickness of 0.2µm. The pattern is etched into the signal layer using the previous technique described in section 3.1.5.

3.1.7 Second Sacrificial Oxide Growth and Patterning

To form the mechanical layer oxide which is grown to 2µm, called SAC2, using the previously used process described in 3.1.2. It is patterned using photoresist and etched using an isotropic wet etch of Buffered Hydrofluoric Acid, etching at about 100nm a minute [12;89,160-162].

3.1.8 Mechanical Layer Formation and Patterning

The mechanical layer is grown using the technique described in 3.1.3 to 2µm. This layer is patterned and etched using the process described in 3.1.5.

3.1.9 Release Sacrificial Oxides

To make the device usable, it needs to be released from its carrier wafer and the formed sensor needs to be released from the confines of the grown oxide. The device and wafer is submerged in Buffered Hydrofluoric Acid. The completed substrate wafer is discarded and the final sensor device is complete. The final device side profile is depicted in Figure 21.

Figure 21 Released Silicon Carbide Strain Sensor

3.2 Silicon Carbide Double Ended Tuning Fork resonant Strain Transducer

The double ended tuning fork could be made into a high temperature strain sensor. This device is favorable because it uses capacitance instead of resistance. It can be fabricated with a silicon carbide process making resistant to extreme environments. This

section discusses using silicon carbide as a material to fabricate the double ended tuning fork strain sensor.

3.2.1 Silicon carbide as a material for the Double Ended tuning fork (DETF).

Double ended tuning forks (DETF) are also known as Resonant Sensors [22:841-845]. They can be applied to measuring strain. Silicon double ended tuning fork strain sensors have very high resolution or it can resolve about 0.11 micrometers [1;22:841-845]. Silicon based devices are not suited for high temperatures, because the silicon material properties degrade at temperatures greater than 500°C [1]. Electrical properties of silicon cannot operate extendedly above 150°C [2:643-646]. Using silicon Carbide to produce a double ended tuning fork strain device is a possible option. It is also possible to manufacture the sensor directly onto the surface of the strained material.

The Silicon carbide resonant strain sensor operates just like the resonant strain sensor described in Section 2.3. Although one built from silicon carbide allows for many advantages to include: increased temperature operation, high radiation exposure, corrosive media, and large impact survivability [1].

3.3 Silicon Carbide Capacitive Strain Sensor

Resonant strain sensors have the ability to measure strain greater than 0.11µm [1], but lack the ability to measure larger surface areas, which makes it not usable for hypersonic vehicles which require large surface area strain measurements [11]. A newly developed strain sensor is designed and tested, which takes the interdigitated finger concept and the capacitive effects are measured.

3.3.1 New Capacitive Strain Sensor

A new sensor design which can allow an increase in capacitance across the device

is designed.   Also the device should be scalable to allow larger measuring areas depending on stresses expected in the measuring material and configuration.   First start with the double ended tuning fork and modify it by increasing the number of interdigitated fingers and eliminating the moving shuttle.   When the movable shuttle is eliminated the device's requirement to tune to the proper frequency would be eliminated, allowing for a passive measuring of capacitance.   By keeping the interdigitated fingers the simple capacitance model of a parallel plate makes it reasonably simple device in operation, this is why it is chosen.   Figure 22 show the modified version of the strain sensor.   To increase capacitance or the measuring surface or geometry, simply increase the quantity of interdigitated finger sets, or increase the quantity of the axial finger sets, this is shown in Figure 22.   Each axial finger set is connected to subsequent axial finger sets.   Each interdigitated finger sets is fixed to the surface of the substrate at the anchor end.   The fabricating surface, also considered the flexible backing material, must be minimized to allow the transmission of the measuring surface's strain to the device.   This type of design has not found to been used in the manner, making it a unique sensor at which the strain sensing area can be increased based on requirements that fit the situation.
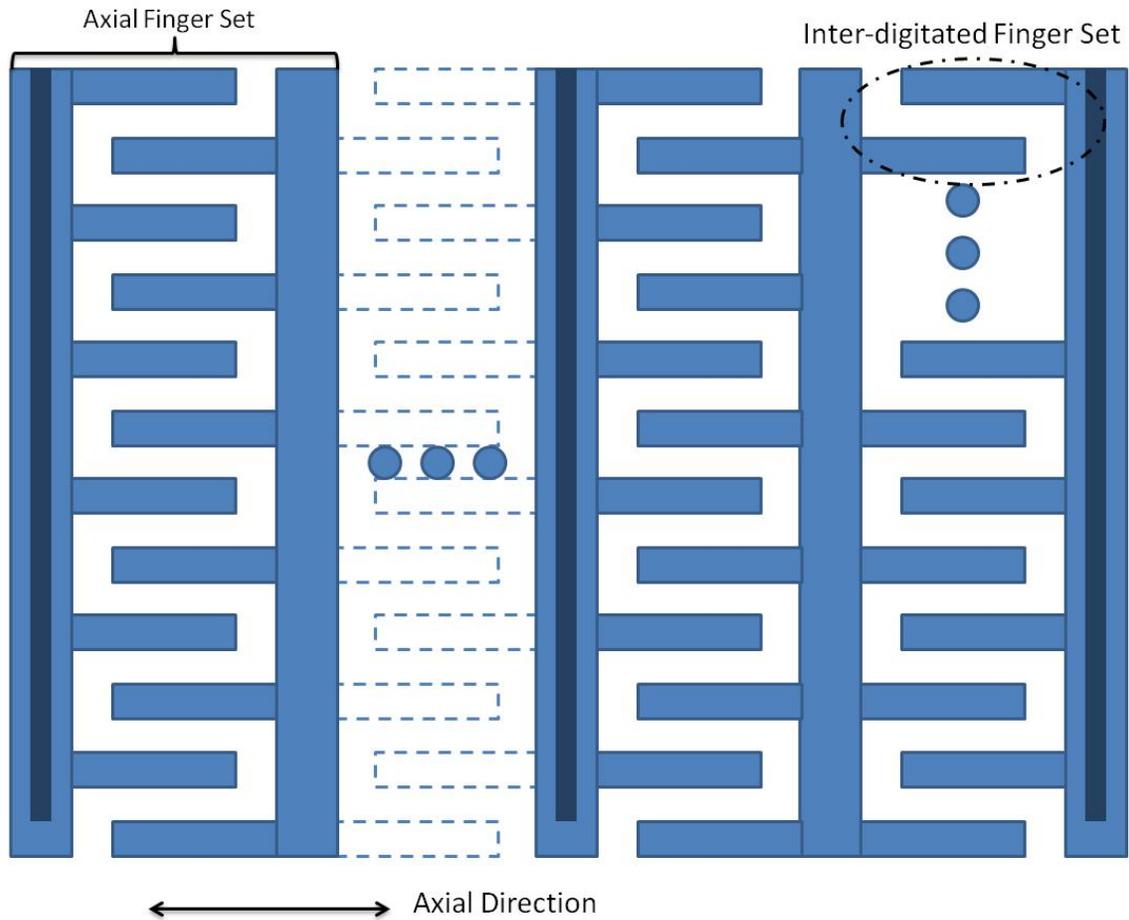
Figure 22 Modified Silicon Carbide Capacitance Strain Sensor

3.4 Mathematical Model Testing

To model the system mathematically gives an opportunity to prove the sensor's ability as a capacitive strain sensor. This section goes through the development of mathematical formulas used to verify operation of each model including, interdigitated finger set, midsize model, and the proposed full size model for use during future testing.

3.4.1 Capacitance model of interdigitated finger

To mathematically model the capacitance between the interdigitated fingers the device must be broken up into smaller bits. A close up of the interdigitated fingers,

38

shown in Figure 23, depicts regions of interest. These regions are; purple, yellow, red, green, and orange.
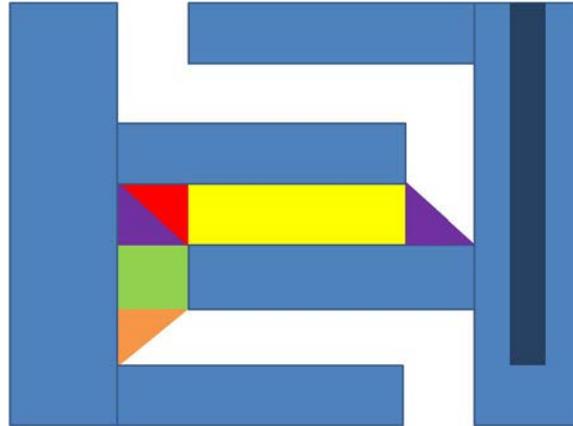
Figure 23 Interdigitated Fingers with Broken Down Regions of Capacitance

Variable breakdown is shown in Figure 24 and Figure 25. L_S, is the axial strain length, which has a breakdown found in equation (16). L_T is the length of one interdigitated finger. W_T is the width of the interdigitated finger. T is the thickness of the silicon carbide mechanical layer.

$$L_S = L_0 + \Delta L \qquad (16)$$
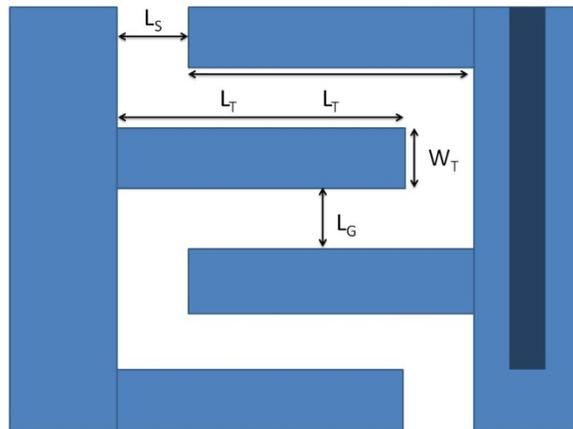
Figure 24 Interdigitated Variables
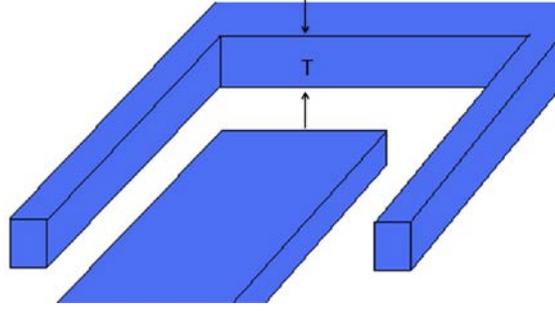
Figure 25 Isometric View of the Interdigitated Finger's Variables

Capacitance in the yellow region is found using equation (17). Capacitance in the green region is found using equation (18). The red, purple and orange regions are difficult to mathematically model. They however are considered of negligible capacitance, due to fringe effects, depicted in Figure 15. This is mostly because the contact size of one end of the parallel plate capacitor is infinitesimally small when compared to the other side. These regions are not mathematically modeled here.

$$C_{YELLOW} = \frac{\varepsilon LW}{d} = \frac{\varepsilon_r \varepsilon_o [L_T - (L_0 - \Delta L)](T)}{L_G} \tag{17}$$

$$C_{GREEN} = \frac{\varepsilon LW}{d} = \frac{\varepsilon_r \varepsilon_o (W_T)(T)}{(L_0 - \Delta L)} \tag{18}$$

Variables and material properties used for the theoretical device to be tested are summarized in Table 3. These parameters are selected based on manufacturability at the Air Force Institute of Technology's clean room fabrication limitations, based on silicon not silicon carbide. Also thickness limitations of silicon carbide layers are based on fabrication processes discusses in 2.7 Silicon Carbide Manufacturing Techniques and references [24:1109-1114;23:2-9]. Also sacrificial layers are determined based on fabrication processes and etch rates based on references [9:43-44;11]. The number of

40

axial finger sets and interdigitated finger sets are determined by the straining surfaces measuring requirements.

Table 3 Silicon Carbide Capacitive Strain Variable Quantities and Material Properties

Silicon Carbide Capacitive Strain Attributes			
Discription	*Varible*	*Value*	*Unit*
Axial strain length	L_S	150	μm
Length of one inter-digitated finger	L_T	150	μm
Length of gap between inter-digitated fingers	L_G	3	μm
Width of the inter-digitated finger	W_T	3	μm
thickness of the silicon carbide mechanical layer	T	2	μm
Original Length of Axial Strain Gap	L_O	10	μm
Axial strain length delta	ΔL	variable	μm
Axial finger set quantitiy	N_{AFS}	variable	n/a
Inter-digitated finger set quantity (in one Axial Finger Set)	N_{IDFS}	variable	n/a
Carrier Substrate Thickness	T_C	300	μm
SiO2 Sacrifitial Layer 1	T_{SAC1}	3	μm
SiC Substrate Flexiable Backing	T_{SiCB}	16	μm
SiN Passivation Layer Thickness	T_{SiN}	0.2	μm
SiC Signal Trace Layer	T_{SiCS}	0.2	μm
SiO$_2$ Sacrifitial Layer 2	T_{SAC2}	2	μm
SiC Mechanical Layer	T_{SiCM}	2	μm

3.4.2 Capacitance as it Relates to Strain and Force

Using Equations (17) and (18) we can figure out the total capacitance due to overall or average strain over the entire sensor. Equation (19) and (20) shows the interdigitated finger set total capacitance. Equation (21) shows the total capacitance for the entire sensor, which includes N_{AFS}, number of Axial Finger Sets, and N_{IDFS}, number of interdigitated finger sets.

$$C_{Fingerset} = C_{Yellow} + C_{Green} \qquad (19)$$

$$C_{Fingerset} = \frac{\varepsilon_r \varepsilon_o [L_T - (L_0 - \Delta L)](T)}{L_G} + \frac{\varepsilon_r \varepsilon_o (W_T)(T)}{(L_0 - \Delta L)} \tag{20}$$

$$C_{Strainsensor} = N_{AFS} * (N_{IDFS} * C_{Fingerset} + C_{Green}) \tag{21}$$

As shown, the capacitance is dependent on ΔL, or change in length, which comes from strain, ε. Equation (22) shows the form of strain, from Section 2.2.2, L is the overall strain sensor length. Overall sensing part, not including anchors and non sensing features, original strain sensor length can be found by adding the number of axial finger sets over the length of the sensor, as shown in equation (23).

$$\varepsilon = \frac{\Delta L}{L} \tag{22}$$

$$L = N_{AFS}(L_T + L_0) \tag{23}$$

To get strain, a relationship needs to be developed between strain, stress, and change in length. Using equations (5), for force on an area produces stress, (2), strain at a given stress, and (22), strain as it relates to change in length, creates, equation (24). Equation (24) shows the relationship between force, stress, and strain. Area refers to the loaded surface or width of the device times the thickness of the substrate (T), σ refers to stress per unit area, ε refers to strain, and E refers to Young's Modulus.

$$F = Area * \sigma = Area * \varepsilon * E \tag{24}$$

Load is applied to the interdigitated finger set model as a distributed load throughout the surface of between the ends of the substrate. One end of the substrate is "fixed", load reaction (fixed) end, and the other the load is introduced in the substrate

Load Introduced End, which is depicted in Figure 26. This allows equation (24) to be rewritten as equation (25), force uniformly distributed over the loaded surface area.

$$\frac{F}{Area} = \sigma = \varepsilon * E = \frac{\Delta L}{L_0 + L_T} * E \tag{25}$$
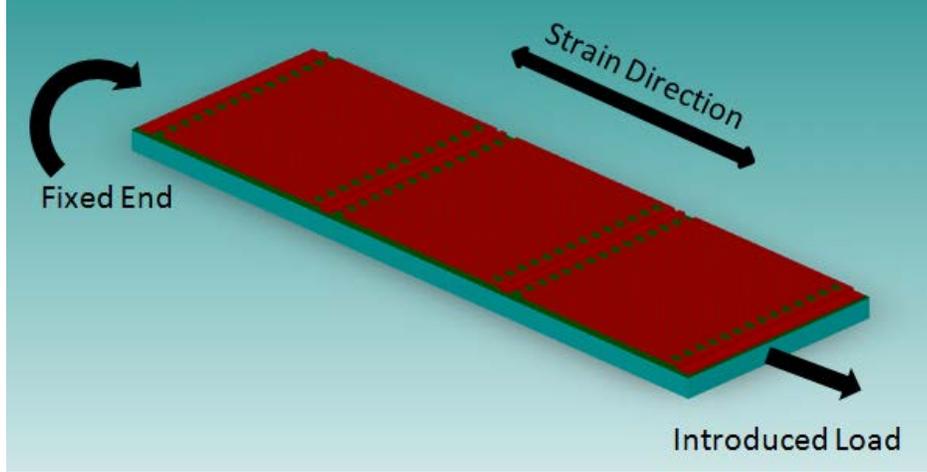
Figure 26 Loading Scheme of Strain Sensor

Equations (19), (20), (21), (22), and (23) are adjusted for the exact geometry of the interdigitated finger sets and rewritten as equations (26), (27), and (28). Equation (26) is defined as the change in length, or displacement.

$$\Delta L = (L_0 + L_T) * \frac{F/Area}{E} \tag{26}$$

Equation (27) is the capacitance of the finger set model.

$$C_{Fingerset} = \frac{\varepsilon_r \varepsilon_o [L_T - (L_0 - \Delta L)](T)}{L_G} + \frac{\varepsilon_r \varepsilon_o (W_T)(T)}{(L_0 - \Delta L)} \tag{27}$$

3.4.3 Interdigitated Finger Set Sensing Element Mathematical Model

To determine if a sensor can be fabricated using the interdigitaged finger set sensing elements. The interdigitated fingers need to be mathematically modeled. The L-Edit© layout has been drawn of the interdigitated finger sets and is shown in shown in Figure 27.
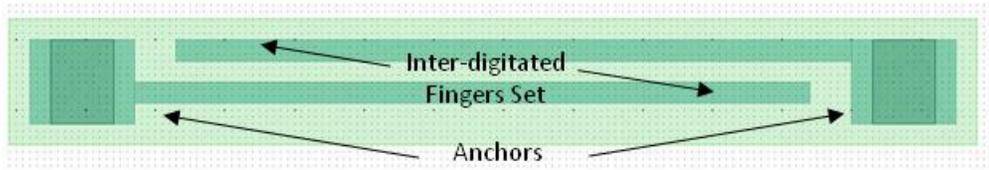
Figure 27 L-Edit© Drawn Interdigitated Finger Layout

Using Equation (27) and Equation (18), Equation (28) is developed for the interdigitated finger set layout.

$$C_{Strainsensor} = C_{Fingerset} + \frac{\varepsilon_r \varepsilon_o (W_T)(T)}{(L_0 - \Delta L)} \qquad (28)$$

3.4.4 Intermediate "Midsized" Model Sensing Element Mathematical Model

To prove that the model can be expanded using increasing amounts axial finger sets and interdigitated fingers, a mathematical model is developed for the midsized. The midsized design has 3 axial finger sets, and 28 interdigitated finger sets. Figure 28 depicts the L-Edit© layouts.
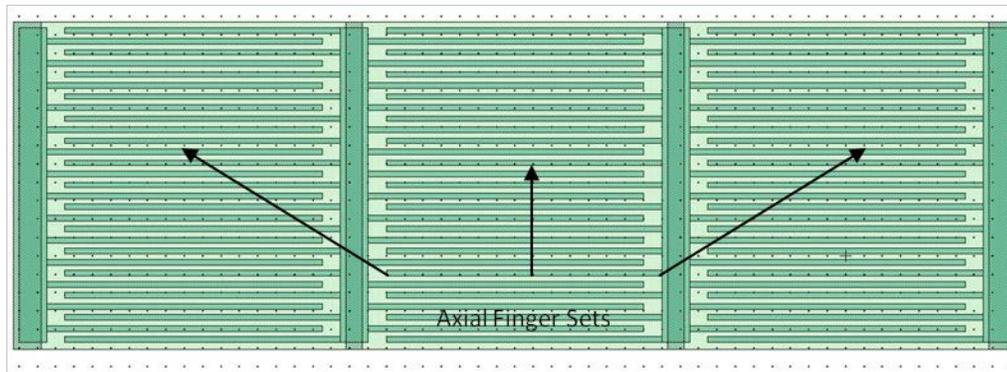
Figure 28 Mid Sized L-Edit© Layout

As stated before, the load is applied to the model as a distributed load to the surface of each end of the substrate. Equation (25), force over the loaded area, can also be used for the midsized model. Equation (26), delta L, is also used for the midsized model. Equation (27), finger set capacitance is also used for the midsized model. The only

difference from the interdigitated finger set model is how the sensor capacitance is determined. Equation (29) shows that the strain sensor capacitance, which includes the number of interdigitated finger sets, $N_{IDFS} = 28$, and the number of axial finger sets, $N_{AFS} = 3$.

$$C_{Strainsensor} = N_{AFS}\left(N_{IDFS} * C_{Fingerset} + \frac{\varepsilon_r \varepsilon_o (W_T)(T)}{(L_0 - \Delta L)}\right) \quad (29)$$

3.4.5 New Capacitive Model Sensing Element Mathematical Model

The midsized can be expanded to allow large sensing elements for various layouts. The number of axial finger sets and interdigitated finger sets can be increased, using equation (29).

3.5 Finite Element Modeling Testing

The new capacitive strain sensor design has been selected using the variables in Table 3. Using these values, an L-Edit[©] layout was developed and tested using material properties from [4:5-12]. A schematic is developed and drawn in L-Edit[©], and then the device is modeled and simulated using Coventorware[©]. Basics of finite element simulation are discussed and a Mesh study is performed on the interdigitated finger set model.

3.5.1 Finite Element Simulation Basics

Finite element simulation software uses numerical solutions of simplified equations to find approximate solutions of partial differential and integral equations. To explain this, a simple explanation is given. Given a volume of electromechanical elements, from a device is broken into smaller volumes of electromechanical elements. The small volume electromechanical elements interact with its neighboring elements. This allows

the approximation or average physical approximation of the whole element, instead of breaking down each interaction with neighboring atoms. The larger the element is, the fewer amount of equations need to be processed for the complete volume. If the volume is too large, the equations become too simple and accuracy is affected. To give a simple example, assume a body is affected by a system of forces, shown in Figure 29. If that body is broken up into smaller elements, forces between each element contributes force lines on each free body diagram, shown Rudimentary in Figure 29. More free body diagram of force equations are created and how those forces act on the internal of the body can be determine. If the elements are shrank down enough the distribution of stress within the object can be realized.
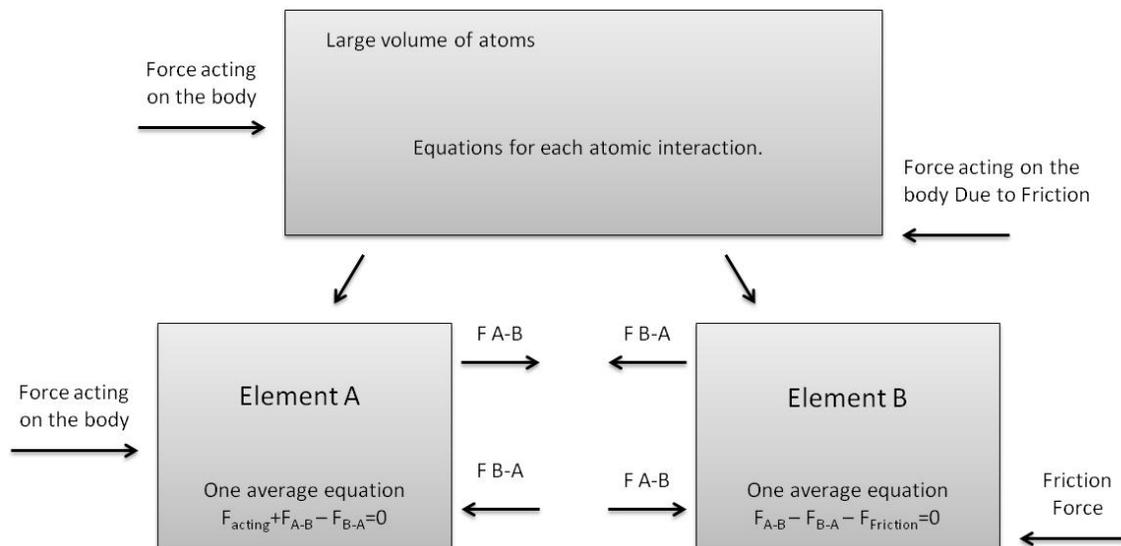

Figure 29 A Rudimentary Example of a Finite Element Analysis Tool

3.5.2 Mesh Study

The small electromechanical elements of the model have to be chosen with three parameters in mind. The first parameter is geometry. There are several options for element shapes. Chosen for the interdigitated finger set is the "Manhattan Bricks"

element shapes. The "Manhattan Bricks" shape is rectangular, and gives three degrees of freedom, or three variations of element sizes. The second parameter is size, or x, y, and z of the individual Manhattan brick elements. The Coventorware$^{©}$ tutorial software gives suggestions on how the element sizes should be varied. First size the initial block size such that it maximizes the element size to the structure tested, x. Second divide those numbers by two for the next varied size, x/2. Third divide the original numbers by four, x/4. The third parameter which could be varied is time. Element size and shape effect time. With a fixed geometry, size can be varied, if the size of the element is shrank the accuracy of the analysis is increased, but the time to execute the analysis also increases. Figure 30 shows the varied element sizes and their execution time performed on the interdigitated finger set. As the size is decreased, the time to execute is longer, but the accuracy is greater. The interdigitated finger set with "Manhattan Bricks" Element shapes and with element size of x=3, y=3, and z=3 is shown in Figure 32, called a meshed model or model mesh or simply mesh. The ideal size of the mesh can be as large as 6 micrometers, any smaller will only allow incremental accuracy improvements with an increased in time. Table 4 depicts the mesh size and execution time. From this table the element size of 3 micrometers allows for an increase in accuracy with a small increase in execution time.
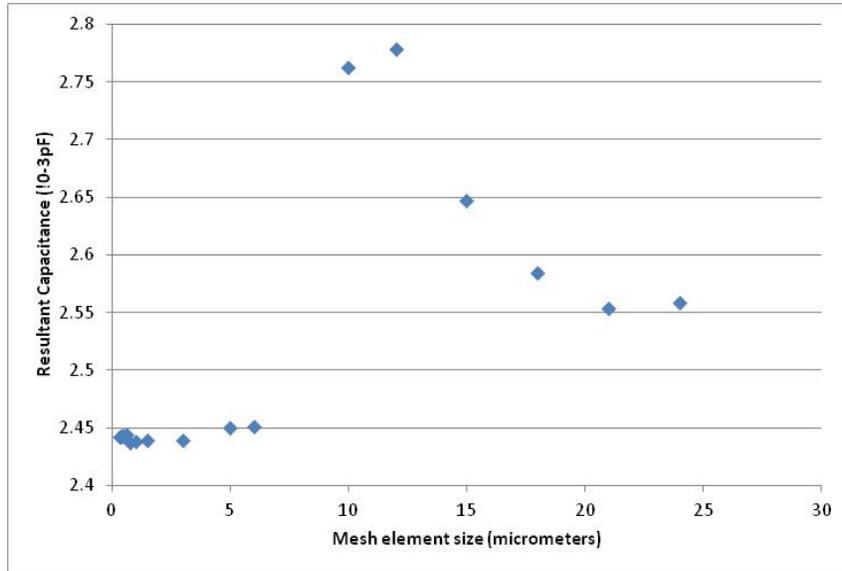
Figure 30 Resultant Capacitance as Mesh Element size is Varied

Table 4 Mesh Element Size and Execution Times

Element (X,Y,Z)	Time to Execute
0.333	43
0.375	28
0.42	23
0.5	18
0.6	9
0.75	9
1	6
1.5	5
3	5
5	2
6	2
10	2
12	2
15	2
18	2
21	2
24	2

3.5.3 Coventorware© Finite Element Modeling and simulation of the Interdigitated Finger Set

To determine if a sensor can be fabricated using the interdigitated finger set sensing elements. The interdigitated fingers need to be simulated using a finite element software. Using these values, an L-Edit© layout was developed and tested using material properties from [4:5-12], and is simulated using Coventorware©. L-Edit© is custom built MEMS software program developed by Tanner EDA© to layout, or draw, MEMS devices [19]. Coventorware© is a custom built MEMS software written by Coventor© for multiphysics finite element modeling and simulation [5]. Its importing process is depicted in Appendix B using material properties from [4:5-12].

The layout is then opened in the mesh generator part of Coventorware©. When it is opened in the mesh generator software, a three dimensional model is created, shown in Figure 31. The dark green is the nitride layer, the red is the silicon carbide mechanical layer, and the light green is the silicon carbide substrate. The trace layer has been taken out for simplicity, and the oxide has been removed to simulate the release of the process. The meshed model created using a mesh size of x=3, y=3, and z=3 on the interdigitated fingers, the substrate's mesh size is x=3, y=3, and z=10 is depicted in Figure 32. The mesh size of the substrate is larger in the z direction because the strain occurs only in the x direction and not in the z direction, so there is no need to measure in the z direction.
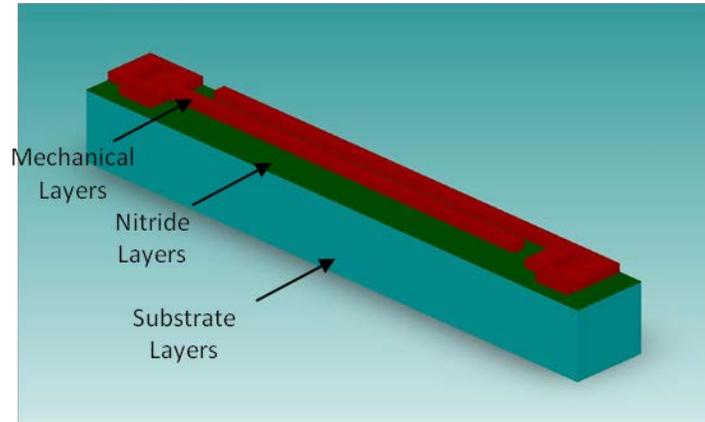
Figure 31 Three Dimensional Model of the Interdigitated Finger Set
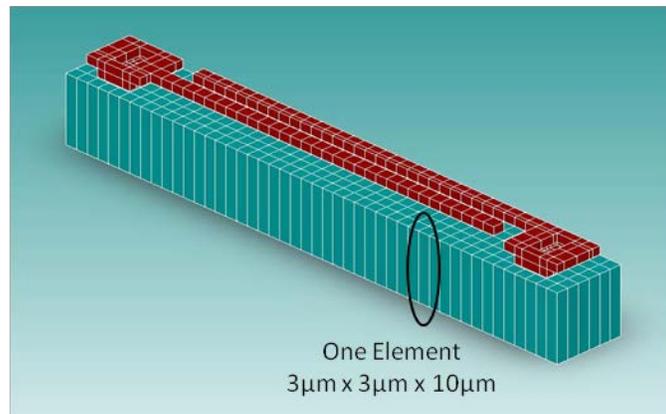
Figure 32 Meshed Three Dimensional Model

3.5.1 Coventorware$^{©}$ Finite Element Modeling and simulation of the Intermediate "Midsized" Model

The layouts are imported into Coventorware$^{©}$ in the same manner as the interdigitated finger set layouts, shown in Figure 33. The three dimensional models are created in the same manner as the interdigitated finger set, depicted in Figure 34. Since the mid model is similar to the interdigitated finger set, the meshed model created using a mesh size of x=3, y=3, and z=3 on the interdigitated fingers, the substrate's mesh size is x=3, y=3, and z=10 is depicted in Figure 35.
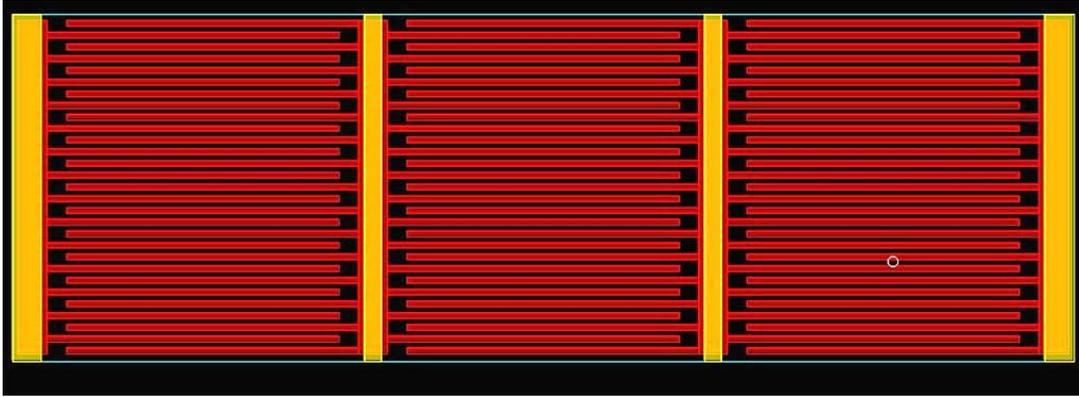
Figure 33 Coventorware© Layout Editor drawing of the Mid Layout
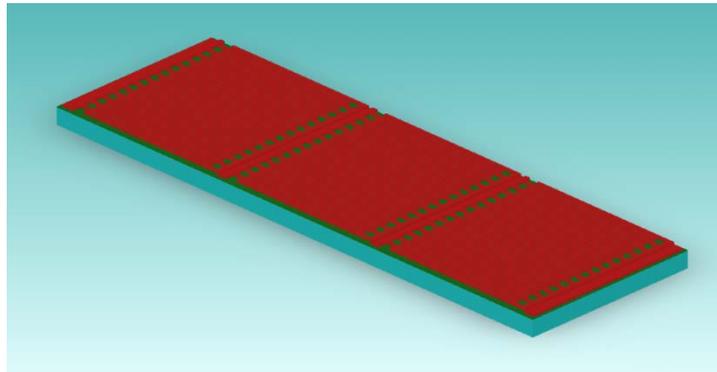
Figure 34 Three Dimensional Coventorware© model of the Mid Layout
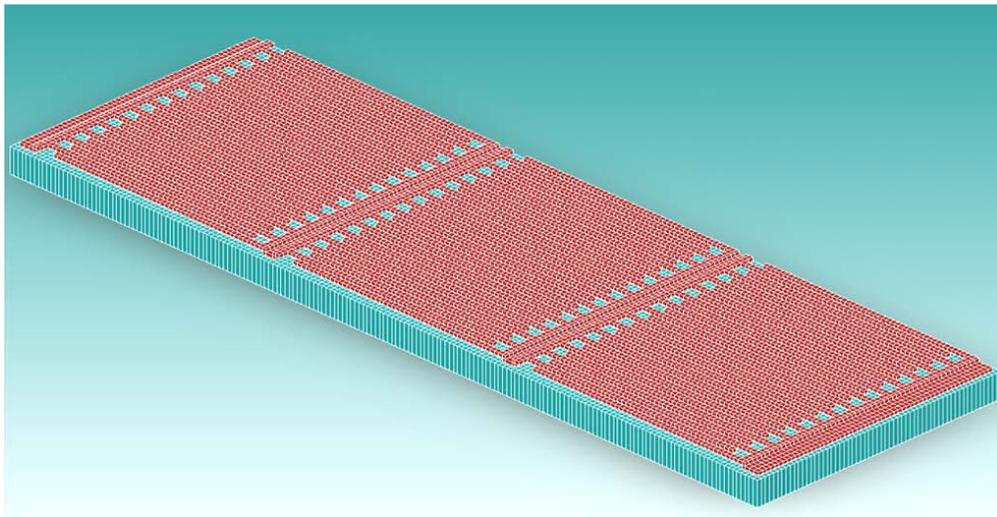
Figure 35 Coventorware© Meshed Model of the Mid Model

IV. Results

This chapter discusses the results of the prescribed testing set forth in Chapter III. Specifically, the interdigitated finger set and midsized model. Each model's mathematical formulas, developed in Section 3.4, are put into Matlab[©] and plots are produced. Also the Coventorware[©] models, developed in Section 3.5, are processed and data along with some three dimensional results are produced.

4.1 Interdigitated Finger Set Model Results

The interdigitated finger set mathematical models are plotted and checked using Matlab[©]. The three dimensional model of the interdigitated finger set is tested using Coventorware[©] mesh model analyzer. The results are presented in this section.

4.1.1 Mathematical Model Simulations

Equation (28) depicts capacitance as length increases. Length increases as force is applied as a uniformly applied force as depicted in equation (25). The results of this length due to force applied is depicted in Figure 36. Load ranging from 0 to $2125\mu N/\mu m^2$ makes change in length vary from 0 to 0.7 micrometers. This force was chosen to get a displacement of 0.7 micrometers to depict the operation of the sensor. This displacement depicts the sensor in use as a strain sensor due to strain at the surface of the straining substrate.

As the length changes due to force, as shown in Figure 36, a change in capacitance occurs, as shown in Figure 37. Load ranging from 0 to $2125\mu N/\mu m^2$ makes capacitance vary from 5.549e-4 picofarads to 5.605e-4 picofarads. This shows that as the substrate is loaded capacitance increases.
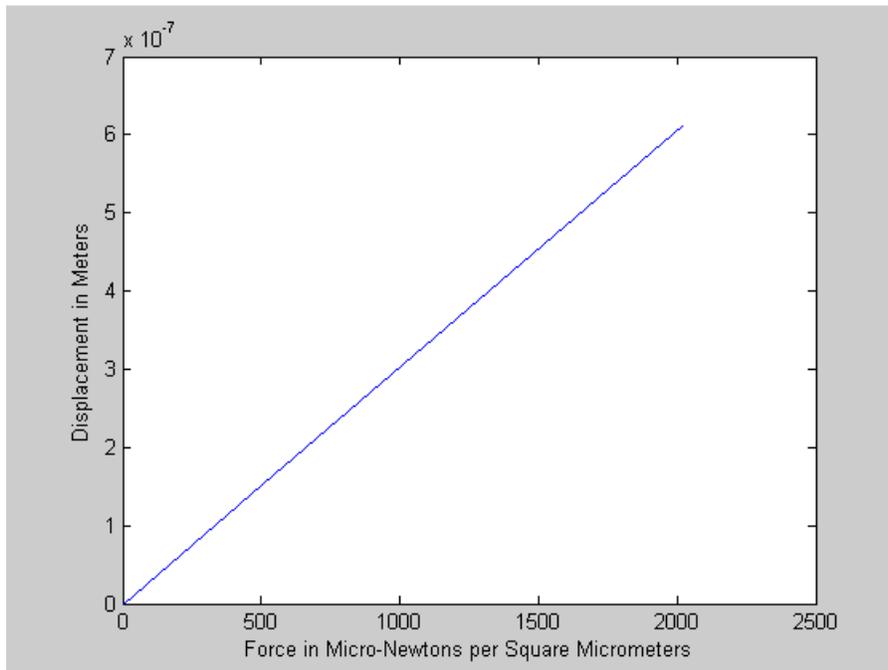
Figure 36 Force versus Displacement for the IDFT Model
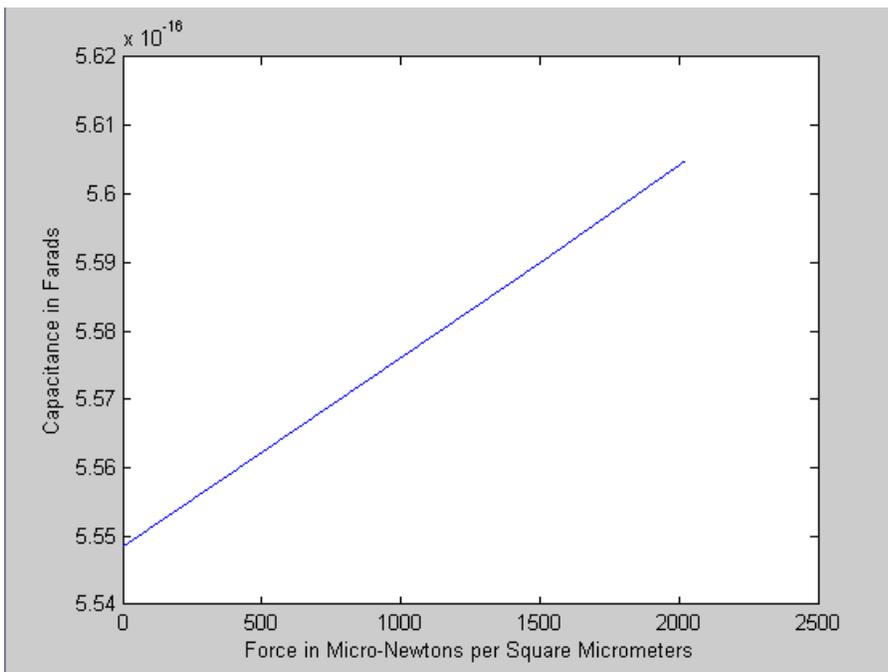
Figure 37 Capacitance Mathematical Plot Results for the IDFT

4.1.2 Coventorware© Simulations

The three dimensional model developed in section 3.5.3 is put through the mesh model analyzer software, but to perform a mesh analyzer some constraint boundary conditions need to be put together. The interdigitated finger set is comprised of 2 contacts, attached to the substrate via anchors. The first contact, or low voltage contact, is named "Negative Finger". The second contact, or high voltage, is named "Positive Finger". These names are shown on the double ended tuning fork in Figure 38.
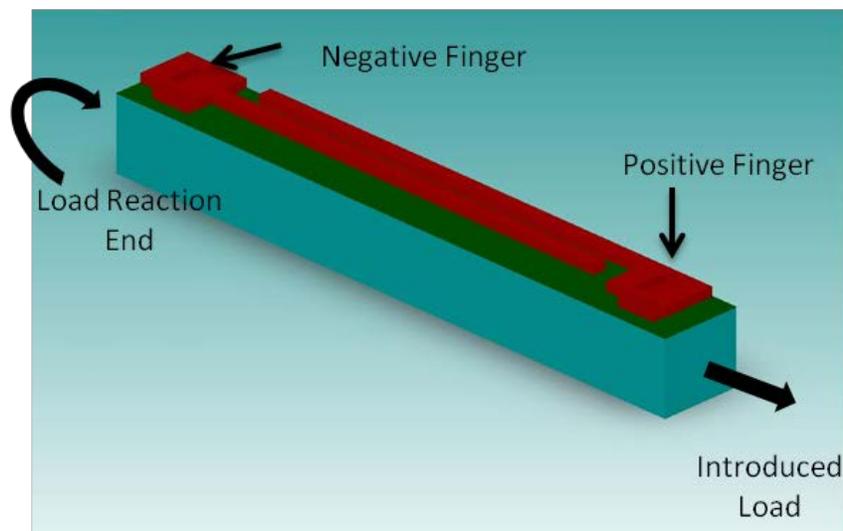
Figure 38 Load Introduction Scheme for the Interdigitated Finger Set

A voltage is applied in Coventorware© between the positive and negative fingers to allow a charge to build up. Figure 39 depicts charge building up on the interdigitated finger walls at no load, signified as yellow and red. This shows that the unloaded finger set builds a charge. Equation (30) shows the formula for charge, q, as voltage multiplied by capacitance. This depicts the charge distribution on the surface of the unloaded sensor interdigitated fingers surfaces.

$$q = V * C \qquad (30)$$
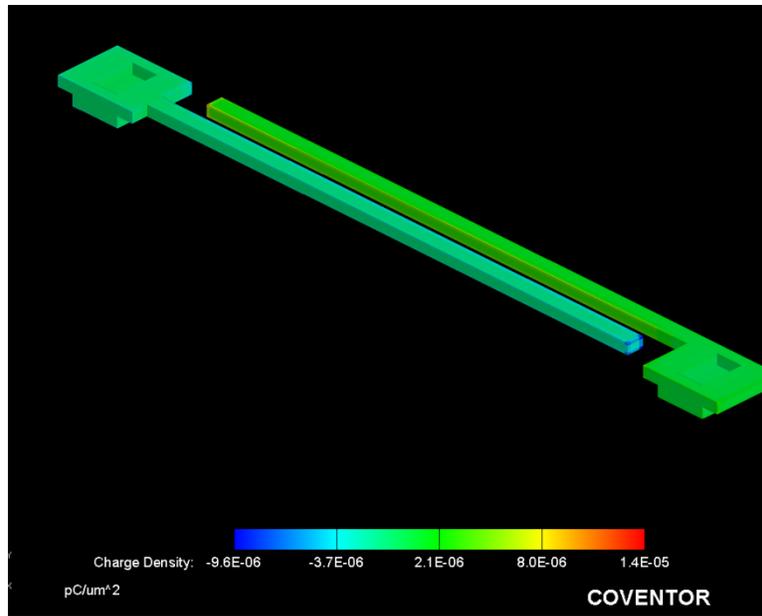
Figure 39 Charge Buildup on the interdigitated finger walls

To make Coventorware[©] think the contact anchors, shown in Figure 38 the color red, are attached to the substrate, shown as the color cyan, the linkage boundary conditions tool is used. The negative finger anchor bottom is "Tied Link" to the ground top, which means the two surfaces are "fused" during all simulations, at the position put forth in the L-Edit[©] layout. The positive finger anchor bottom is "Tied Link" to the ground top at its position put forth in the L-Edit[©] layout.

To apply a load to the interdigitated finger set one end must be fixed and the load is applied to the other end. To do this the faces at which the load is applied and the fixed end have to be named. The fixed end is called the "Load Reaction End", because it "reacts" against a stationary position. The end that the load is applied to is called the "Load Introduction End". Figure 38 also depicts how the load is applied and fixed end.

Three forces are simulated in Coventorware[©] for the interdigitated finger sets, $0\mu N/\mu m^2$, $531\mu N/\mu m^2$, and $1062\mu N/\mu m^2$.

Figure 40 depicts the results of the distributed load across the load introduction end at $531\mu N/\mu m^2$. It shows that from the reaction to the load introduction ends there is a change in length of $0.22\mu m$.
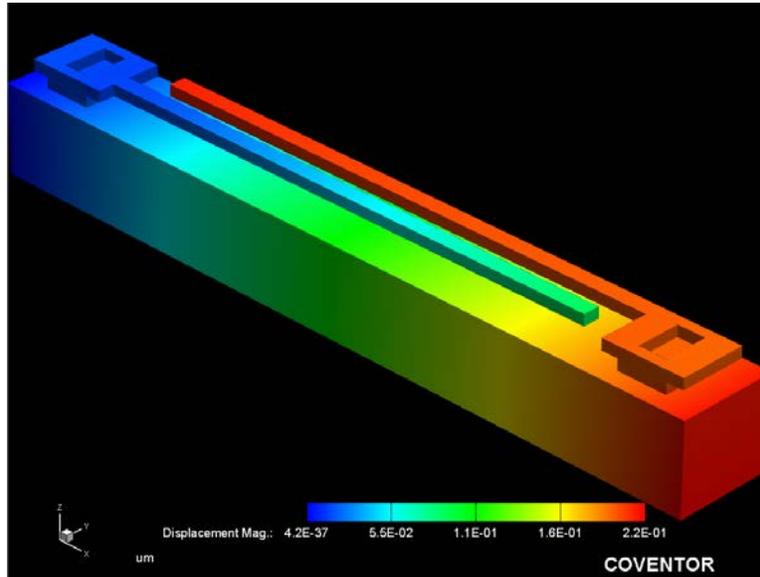
Figure 40 Coventorware[©] Displacment Results at $531\mu N/\mu m^2$

Figure 41 depicts the results of the distributed load across the load introduction end at $1061\mu N/\mu m^2$. It shows that from the reaction to the load introduction ends there is a change in length of $0.43\mu m$.
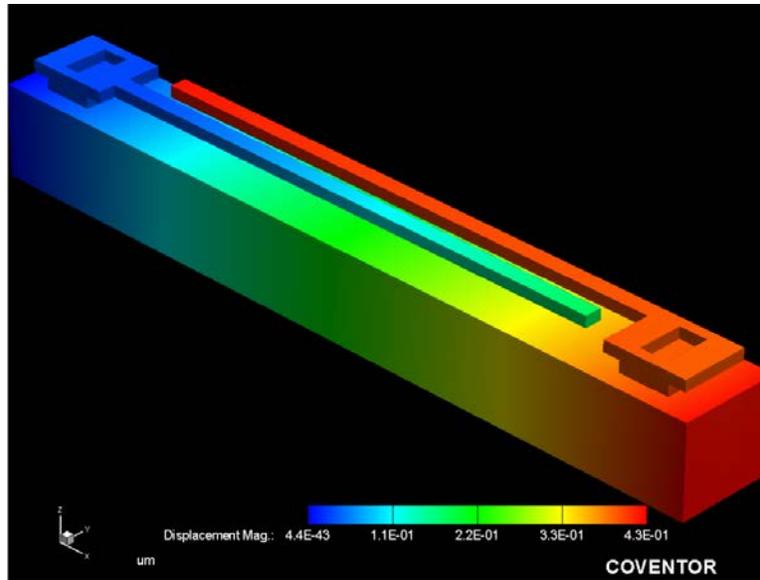
Figure 41 Coventorware$^{©}$ Displacement Results at $1062\mu N/\mu m^2$

When the interdigitated finger set model is subjected to load, and stress exists within the material. Figure 42 shows the stress distribution within the interdigitated fingers. The load introduction end is stationary as a part of the testing so stress is concentrated here. The substrate shows a uniform stress density of about 460 MPa. Stress concentrates at the negative and positive anchors of about 800 MPa. It also shows that there is no stress within fingers.
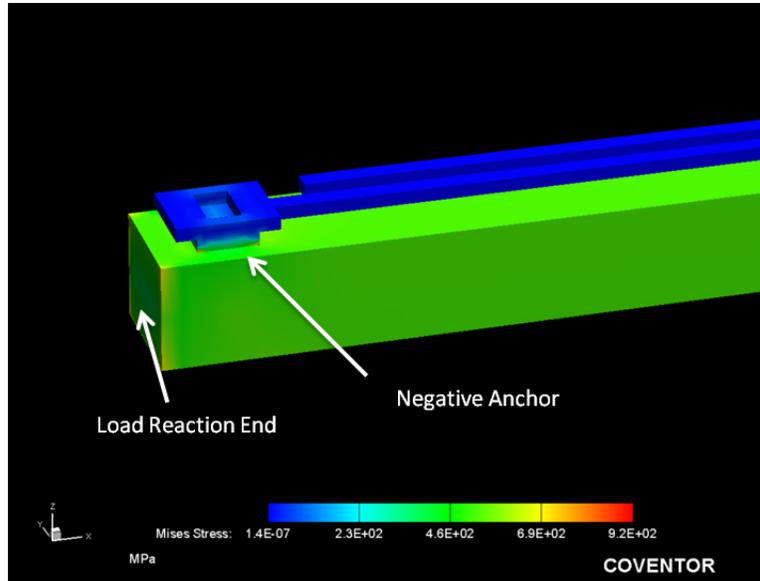
Figure 42 Coventorware© Stress Results on the Load Reaction End and the Negative Anchor at

$$531\mu N/\mu m^2$$

4.1.1 Summary of the Interdigitated Finger set Model

The results of change of length from Coventorware© and the mathematical models are summarized in Table 5. As shown the mathematical results are very close to the Coventorware© results. Displacement from mathematical model is a little different than the displacement within the substrate. The displacement measurement in Coventorware is measured from the load reaction end to the load introduction end. The displacement estimate in the mathematical model is measured from negative anchor face to positive anchor face.

58

Table 5 Summary of Displacement for Interdigitated Finger Set Tests from the Mathematical and

Coventorware© Models

delta L Summary		
Load	Mathmatical Results	Coventorware© Results
µN/µm	µm	µm
No Load	0	0
531	0.1534	0.22
1062	0.3067	0.43

The results of change of capacitance from Coventorware© and the mathematical models are summarized in Table 6. As shown the mathematical model is an order of magnitude off from the Coventorware© model. Coventorware© electrostatic models are more strengient then the models developed in section 3.4. The model takes into count the capacitance developed from the surface of the substrate to the fingers. It also figures in the capacitance within the finger structure and parasitic capacitance from the mounting elements within the anchors to the surface of the substrate. If the results are normalized, or divided by the no load magnitude, we can see that the delta capacitance is fairly close. The difference in the normalized capacitances could be due to the slight difference in how the delta L is realized.

Table 6 Summary of Capacitance for the Interdigitated Finger Set Tests from the Mathematical

and Coventorware© Models

Capacitance Summary				
Load	Mathmatical	Mathmatical	Coventorware©	Coventorware©
µN/µm	pF	Normalized	pF	Normalized
No Load	5.55E-04	0.0000	2.43878E-03	0.0000
531	5.56E-04	0.0023	2.44330E-03	0.0019
1062	5.58E-04	0.0049	2.44786E-03	0.0037

The results show that the interdigitated finger set is a good parallel plate capacitor design for measuring strain using the capacitive effect, even though the magnitudes are fairly small, on the order of 1e-3pF, The simple mathematical models developed in section 3.4 are a close representation of the general operation and will allow a reasonable relationship to what Coventorware© depicts. It allows a normalized increase of capacitance during the increase of strain due to a uniformly distributed load. This model is a good model to use. Because of symmetry the interdigitated finger set results can be multiplied by the quantity of interdigitated finger sets and by the axial finger sets of a given design, to give results of that design.

4.2 Midsized Model Results

The midsized mathematical models are plotted and checked using Matlab©. The three dimensional model of the midsize model is tested using Coventorware© mesh model analyzer. The results are presented here.

4.2.1 Mathematical Model Simulations

Equation (29) depicts capacitance as length increases. Length increases as force is applied as a uniformly applied force as depicted in equation (25). The results of this length due to force applied is depicted in Figure 43. Load ranging from 0 to 2125µN/µm^2 makes change in length vary from 0 to 1.0µm. Load ranging from 0 to 2125µN/µm^2 makes capacitance vary from 6.988e-2 pF to 7.043e-4 pF, as shown in Figure 44.
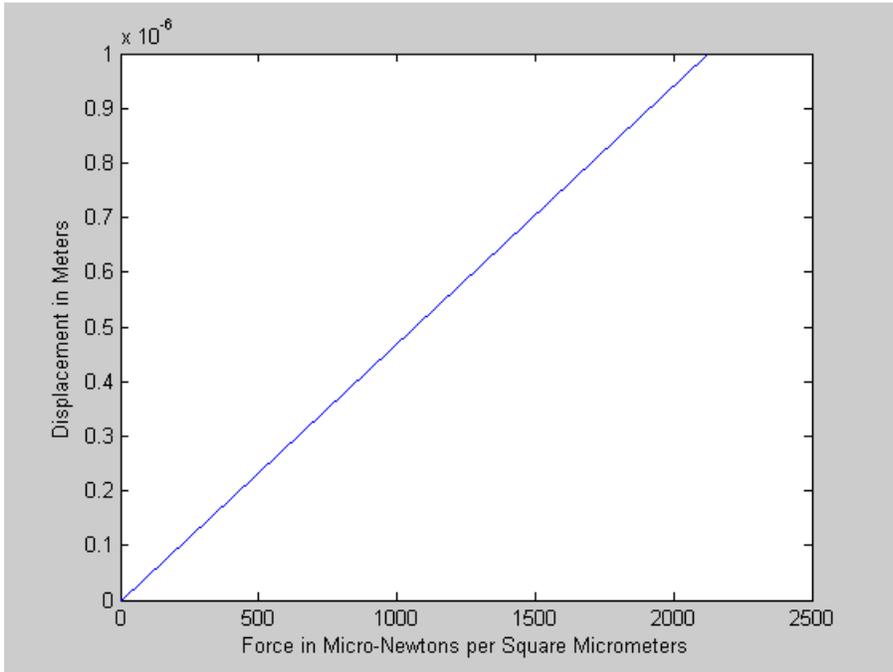
Figure 43 Force versus Displacement for the Midsize Model
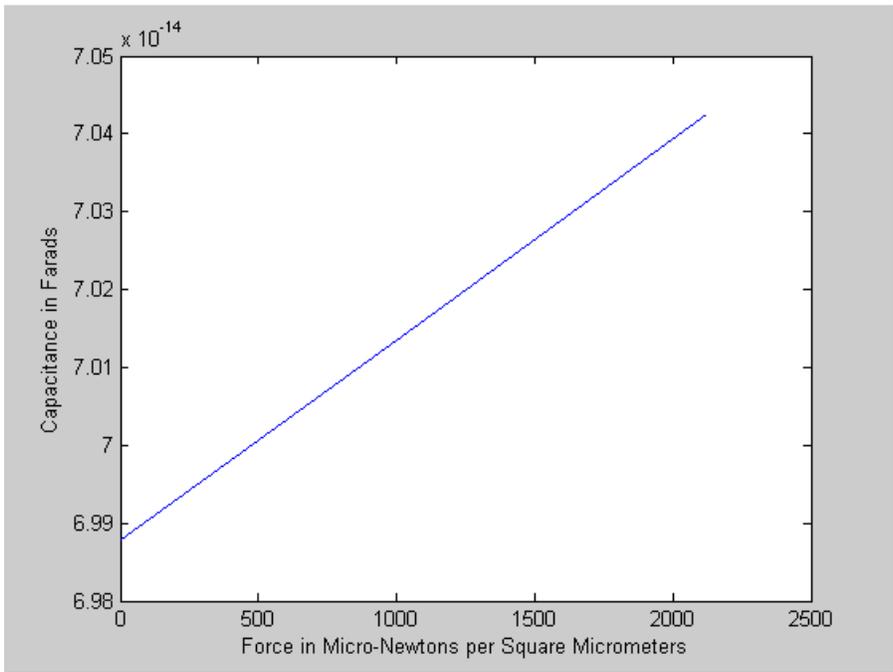
Figure 44 Capacitance Mathematical Plot Results for the Midsized Sensor

4.2.2 Coventorware© Simulations

The three dimensional model is put through the mesh model analyzer software, but to perform a mesh analyzer some constraint boundary conditions need to be put together. The midsized model is comprised of 4 contacts, attached to the substrate via anchors. The first contact is named "Anchor 1". The second contact is named "Anchor 2". The third contact is named "Anchor 3". The fourth contact is named "Anchor 4". These names are shown on the double ended tuning fork in Figure 45.
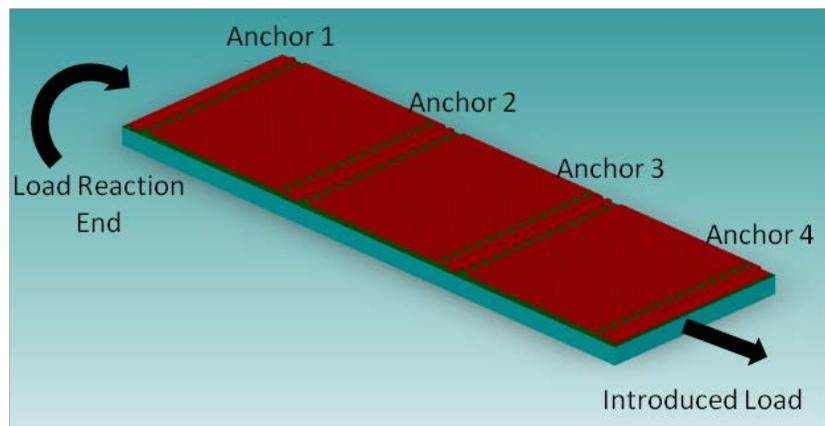
Figure 45 Load Introduction Scheme for the Midsize Sensor

A voltage is applied in Coventorware© between the anchors to allow a charge to build up. 1vDC is applied to anchor 2 and anchor 4, and 0 vDC voltage is applied to anchor 1 and anchor 3. As stated before, this DC voltage differential will create a charge between anchor 1 and 2, anchor 2 and 3, and anchor 3 and 4 thus creating a capacitance between those anchors.

To make Coventorware© think the contact anchors, shown in Figure 45 the color red, are attached to the substrate, shown as the color cyan, the linkage boundary conditions tool is used, each of the anchor bottoms are a "Tied Link" to the ground top,

which means the surfaces are "fused" during all simulations, at the position put forth in the L-Edit© layout.

To apply a load to the midsized sensor one end must be fixed and the load is applied to the other end. To do this the faces at which the load is applied and the fixed end have to be named. The fixed end is called the "Load Reaction End", because it "reacts" against a stationary position. The end that the load is applied to is called the "Load Introduction End". Figure 45 also depicts how the load is applied and fixed end.

Three forces are simulated in Coventorware© for the interdigitated finger sets, zero micronewtons per square micrometer and $1061\mu N/\mu m^2$. Figure 46 depicts the results of the distributed load across the load introduction end at $531\mu N/\mu m^2$. It shows that from the reaction to the load introduction ends there is a change in length of 1.8µm.
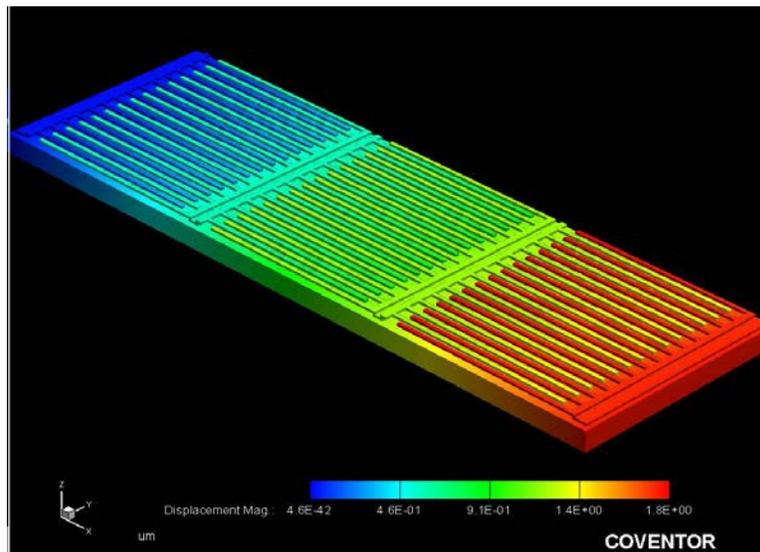
Figure 46 Coventorware© Displacement Results at 1061 Micronewtons per Square Micrometers for the Midsize Sensor

4.2.1 Summary of the Midsized Sensor Model

The results of change of length from Coventorware[©] and the mathematical models are summarized in Table 7. As shown the mathematical results are a bit off of the Coventorware[©] results. The displacement measurement in Coventorware is measured from the load reaction end to the load introduction end. The displacement estimate in the mathematical model is measured from negative anchor face to positive anchor face which if measured from the L-Edit[©] drawing is about 65µm different. The substrate is still displaced throughout the whole surface. The mathematical model does not account for this, because its only concern is sensing element, or the area under the interdigitated fingers.

Table 7 Summary of Displacement for the Midsized Design Tests from the Mathematical and

Coventorware[©] Models

Displacement Summary		
Load	Mathmatical	Coventorware[©]
µN/µm	µm	µm
No Load	0	0
1061	0.5	1.8

The results of change of capacitance from Coventorware© and the mathematical models are summarized in Table 8, which shows the mathematical model is off from the Coventorware[©] model. If the results are normalized, or divided by the no load magnitude, we can see that the delta capacitance is fairly close. The Coventorware© model takes into count the capacitance developed from the surface of the substrate to the fingers. It also figures in the capacitance within the finger structure and parasitic capacitance from the mounting elements within the anchors to the surface of the substrate. Reference [18], depicts interactions from other interdigitated fingers within an

64

axial finger set, shown in Figure 16. The interactions in electric fields occur from the positive potential to negative potential fingers and from the positive potential fingers to the substrate. Figure 47 also depicts interactions of electric fields between finger 1, positive potential fingers, to fingers 2 and 4 (shown as a "…" to indicate this model can be expanded to include many more fingers), negative potential fingers. Also the same can be said from finger 5, positive, to fingers 4 and 2, negative. As shown in equation (15) electric field is related to charge and capacitance.

Table 8 Summary of Capacitance for the Midsized Design Tests from the Mathematical and Coventorware© Models

Capacitance Summary				
Load	Mathmatical	Mathmatical	Coventorware©	Coventorware©
µN/µm	pF	Normalized	pF	Normalized
No Load	6.988E-02	0.000000	0.2068364	0.00000
531	7.02E-02	0.00386	0.2080181	0.00571
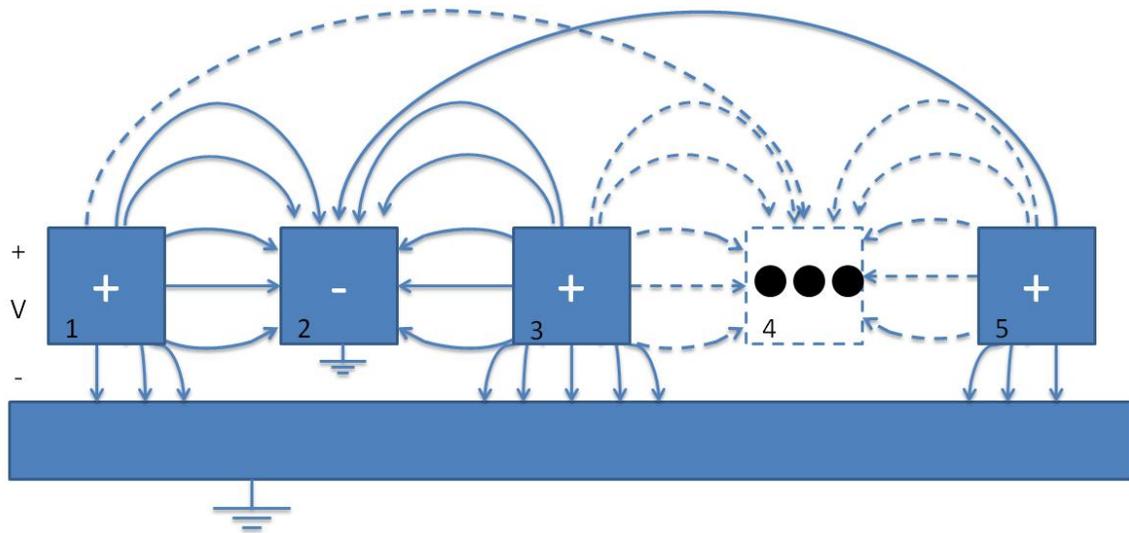
Figure 47 Electric Field Relationship Between Interdigitated Fingers

If the results are normalized, or divided by the no load magnitude, we can see that the delta capacitance is fairly close. The difference in the normalized capacitances could be due to the slight difference in how the delta L is realized.

The simple mathematical models developed in section 3.4 are a close representation of the general operation and will allow a reasonable relationship to what Coventorware© depicts. The midsized model is significantly larger than the interdigitated finger sets. This is shown in the substantial increase in magnitude of capacitance on the order of one pF. This proves that if the amount of interdigitated finger sets is increased capacitance is increased.

V. Conclusions and Recommendations

The Air Force Research Laboratory Air Vehicles Directorate, AFRL/RB, performs research in future generation aerospace vehicles are at the forefront of hypersonic aerodynamic vehicles [21:5915-5924]. When designing hypersonic vehicles, material strength calculations require accurate material properties. This requires experimental analysis of materials based properties which use Hooke's Law of the relationship between material stress and deformation of that material [8:52]. Deformation occurs throughout the material, including at its surface. Measuring deformation at the surface is typically done using a strain sensor. AFRL/RB has the need to measure this deformation at high temperatures, often exceeding 700°C for hypersonic vehicle applications [11].

5.1 Problem statement and Research Objectives

Measuring strain is difficult in high temperature environments, over 700°F, commercial strain sensors were shown to not work within the extreme temperature environments. The objective of this research listed in the following questions has been met:

Why do commercial strain sensors not work in high temperature environment?

How do I design a scalable high temperature strain sensor?

How do I prove the sensor works without manufacturing it?

Within this document a high temperature strain sensor was designed, modeled and simulated using finite element simulation software. Also stress, strain, stress strain relationship was given as a background. Also discussed were measurements using traditional strain sensors, and why they did not work in extreme temperatures. An

alternative design for measuring strain using a double ended tuning fork was discussed. Also discussed is manufacturing processes for making silicon MEMS devices and silicon carbide MEMS devices. A novel strain sensor was designed, and modeled mathematically. This design is a viable solution testing of strain measurements on high temperature hypersonic components, for which the Air Force Research Lab's Air Vehicles Directorate has research programs.

5.2 Conclusions

The development of the new capacitive strain sensor in this paper has been done. The design started through the understanding of how stress, strain, and stress strain relationship. This gives a relationship of force to stress, and from stress to strain or the deformation of a material, shown in section 2.1. The deformation of material can be related to resistance with the change in displacement, ΔL, shown in section 2.2. Foil strain gages were discussed in section 2.2.2 which allows the relationship of gage factor to strain, and the change of resistance. Foil gages were not found to be reliable at high temperatures, as shown in section 2.2.3. One type of alternate strain sensor, the double ended tuning fork resonant strain sensor was shown in section 2.3 to have the ability to measure strain, and due to electric field, capacitance is generated as shown in section 2.4. Making a doubled ended tuning fork resonant strain sensor can only be done using MEMS based processes shown in sections 2.5, 2.6, and 2.7.

The double ended tuning fork resonant strain sensor could have been a candidate for a high temperature strain sensor, using silicon carbide as discussed in 2.6 and 3.2. The double ended tuning fork sensor was found to not fulfill the requirements of a scale able high temperature strain sensor, as discussed in section 3.2 and 3.3. A new strain

68

sensor was designed in section 3.3. This design allowed for a scale able design using the interdigitated fingers that were taken from the double ended tuning fork design, and removing the shuttle mass. The new capacitive strain sensor allows for scalability by adding the ability increase the quantity of interdigitated fingers sets and to the number of axial finger sets, the multiplication of interdigitated finger sets that are multiplied in a transaxial direction. This allows for the sensing element, the interdigitated fingers modeled as a parallel plate capacitor, to be multiplied to fit the sensing length and width requirements of the user.

To answer one of the research objectives, testing the sensor which cannot be manufactured with this research, a mathematical model is created, and Coventorware© simulations are performed. A simple version of the new capacitive strain sensor, the interdigitated finger set model was mathematically modeled in section 3.4.1. Capacitiance as a relation to the change in length, ΔL, was developed in section 3.4.1. The relationship from change in length, ΔL, strain, stress, to force were derived in section 3.4.2 giving a complete model for the interdigitated finger set in section 3.4.3. It shown in section 4.1.1 that as force increased, capacitance increased, proving that this model does work as a strain sensor. This modeled was expanded to the midsized model depicted in section 3.4.4, to prove the scalability of the interdigitated finger set new capacitive strain sensor shown in section 3.4.5. It shown in section 4.2.1 that the increase in interdigitated finger sets and axial finger sets increased the capacitance and the sensing region.

Mathematical modeling shows a lot, but another way this paper proves the new capacitive strain sensor is a viable model for use as a strain sensor was done using a finite

element software package known as Coventorware©, discussed in section 3.5. Using the

silicon carbide fabrication process developed in section 3.1, and the mesh study analysis

in section 3.5.2 Coventorware© can be used to simulate the interdigitated finger set and

the midsize model to compare it to the mathematical model developed. The interdigitated

finger set model was simulated in Coventorware© in section 3.5.3. It showed in section

4.1.2 how charge is distributed in within, and around the model. It shows the distribution

of stress and strain throughout the model. It also shows that the sensor increase

capacitance as strain, stress, or force increases, in section 4.1.2. The mathematical results

and Coventorware© results are compared in section 4.1.1. This shows that the

methodical results and Coventorware© results increase proportionally as strain is applied.

The capacitance magnitude between the mathematical model and the Coventorware©

simulation were different, which is attributed to Coventorware including in its modeling

techniques, electric field which are difficult of mathematically modeling using geometry.

This was also the case with the midsize model, shown in section 4.2.2 and 4.2.1. The

Coventorware© simulation shown as load, stress, or strain, increases capacitance

increases, and when compared to the mathematical approach capacitance increases

proportionally with force applied. Again Coventorware© allows a better model then the

mathematical one derived here, attributed to its fully modeling electric fields.

It has been shown that the interdigitated finger approach satisfied the design

requirements of a capacitive strain sensor that is scalable. It can be deployed using poly

silicon carbide processes allowing it to be used in high temperature environments for

strain sensing.

70

5.3 Recommendation for future work

To realize this design some steps needs to be take to use this sensor as a strain sensor. Full scale testing in a realistic environment needs to be performed. It needs to be characterized using strain as a variable. Techniques for attaching the strain sensor onto its intended sensing surface needs to be explored. Signal conditioning needs to be realized. How does size affect the design? Polysilicon is not an ideal use for temperature related designs, how can it be made using crystalline silicon carbide. How does stress at the interface points from the fingers to the signal lines and to the substrate effect operation, will it break.

The design should be fabricated in order to allow a proof of concept in real life conditions. Upon fabrication the device needs to be tested using temperatures greater than 700°C. There are many ways, using IR heaters, industrial ovens, or quartz lamp heaters. While the device is heated, it needs to be put under a load, verifying the strain sensing functionality.

The affect of size effect operations of the strain sensor needs to be explored.

A sensitivity analysis needs to be performed to determine if the sensor is capable of measuring a sensible resolution.

Characterizing the device can be realized by subjecting the device to various loads and temperatures. This would show a full functionality of the device at changing temperatures.

Signal conditioning is the process of converting one signal into a signal that computers can measure. Since the strain sensor operates on the capacitive effect it is a little difficult to measure using traditional methods. One option could be using the

Wheatstone bridge method. Although this method is commonly used for resistive bridges, it can be adapted to inductive or capacitive bridges.

The more difficult task that lies ahead is attachment of the sensor to the sensed surface. Traditional strain sensors are attached using adhesives, and polymers. Either a high temperature adhesive technique needs to be explored or the strain sensor needs to be manufactured directly onto the sensing surface. The substrate could be the sensing surface instead of the flexible backing that is proposed here.

To see if polysilicon carbide is an ideal material in the sensor's mechanical layer, temperature should be varied as geometry and residual stress are checked. During the mechanical layers fabrication process, at which polysilicon carbide is created, the orientation of the crystalline is of varying orientations within the structure, thus causing internal stresses that may cause variations in the new capacitive strain sensor. To alleviate this problem all together, crystalline silicon carbide could be explored.

When process followers are created to evaporate polysilicon carbide material properties need to be explored. With polysilicon carbide evaporating on polysilicon carbide stress will be concentrated at that interface when the substrate is strained. How much stress will be allowed before the device will "pop off"?

Appendix A: Matlab Code

Appendix A shows the Matlab© code used to determine the results of the

mathematical formulas.

A-1: Matlab Code from the Interdigitated Finger Set Layout Formulas

```matlab
%Weisenberger Thesis Mathematical Modeling IDTF

clear
clear home
clc
%Variables
%Fixed
LT=97*10^-6;      %Length of Interdigitated Fingers (meters)
LG=3*10^-6;       %Gap Distance between interdigitated fingers (meters)
WT=3*10^-6;       %Width of Interdigitated Fingers (meters)
T=2*10^-6;        %Thickness of Silicon Carbide Mechanical Layer (meters)
L0=6*10^-6;       %original length of axial length of finger gap (meters)
ER=1.0;      %Relative Permittivity of Air (unit less)
EF=8.85419e-12;      %Permittivity of Free Space (Farads/meter)
TSiCB=16*10^-6;   %Thickness of Flexible Backing SiC (meters)
LA=15*10^-6;  %Length of the anchor (meters)
LFace=18*10^-6;  %Length of applied load face (meters)
NAFS=1;   %Axial Finger Sets quantity (unit less)
NIDFS=1;  %interdigitated finger set quantity (unit less) Use odd
number to make symmetric
YMSiC=340*10^3;  %Young's Modulus of Silicon Carbide (micronewtons per
square micrometer)
FA=1062;  %Applied Pressure (Micronewtons per square micrometer)
Force=0:FA/2:FA; %Force Applied (Micronewtons per square micrometer)

%Equations
    strain=Force/YMSiC  %strain
    eps=strain;  %conversion to micro strain
    DelL=eps*(LT+L0)      %Delta L relationship with strain
    CY=(ER*EF*(LT-(L0+DelL))*(T))/LG   %Yellow Region Capacitance
    CG=(ER*EF*(WT)*(T))*((L0+DelL).^-1)      %Green Region Capacitance
    CF=CY+2*CG       %Finger Set capacitance
    CS=NAFS*(NIDFS*CF) %Total Strain Sensor Capacitance
    eps2=DelL/(LT+L0) %Verification of Strain

%Plot Mechanism
plot(eps,CS)     %Plot total strain sensor as a function of strain
title('Farads vs. Strain for Interdigitated Finger Set')
xlabel('Strain')
ylabel('Farads')
```

A-2: Matlab Code from the Mid Layout Formulas

```matlab
%Weisenberger Thesis Mathematical Modeling Mid Model

clear
clear home
clc
%Variables
%Fixed
LT=150*10^-6;      %Length of Interdigitated Fingers (meters)
LG=3*10^-6;      %Gap Distance between interdigitated fingers (meters)
WT=3*10^-6;      %Width of Interdigitated Fingers (meters)
T=2*10^-6;       %Thickness of Silicon Carbide Mechanical Layer (meters)
L0=10*10^-6;      %original length of axial length of finger gap
(meters)
ER=1.0;       %Relative Permittivity of Air (unit less)
EF=8.85419e-12;      %Permittivity of Free Space (Farads/meter)
NAFS=3;    %Axial Finger Sets quantity (unit less)
NIDFS=28;   %interdigitated finger set quantity (unit less)
YMSiC=340*10^3;   %Young's Modulus of Silicon Carbide (micronewtons per
square )
TSiCB=16*10^-6;    %Thickness of Flexible Backing SiC (meters)
LA=15*10^-6;   %Length of the anchor (meters)
LFace=178*10^-6;   %Length of applied load face (meters)
FA=2125;   %Applied Force (micronewtons per square micrometers)
Force=0:FA/2:FA; %Force Applied (micronewtons per square micrometers)

%Equations
    strain=Force/YMSiC;   %non micro strain
    eps=strain;   %conversion to micro strain
    DelL=eps*(LT+L0)      %Delta L relationship with strain
    CY=(ER*EF*(LT-(L0+DelL))*(T))/LG   %Yellow Region Capacitance
    CG=(ER*EF*(WT)*(T))*((L0+DelL).^-1)      %Green Region Capacitance
    CF=CY+CG        %Finger Set to region relationship
    CS=NAFS*(NIDFS*CF+CG) %Total Strain Sensor Capacitance

%Plot Mechanism
plot(eps,CS)     %Plot total strain sensor as a function of strain
title('Farads vs. Strain for the Mid Model')
xlabel('Strain')
ylabel('Farads')
```

A-3: Matlab Code from the Final Sensor Layout Formulas

```matlab
%Weisenberger Thesis Mathematical Modeling Final Design

clear
clear home
clc
%Variables
%Fixed
LT=150*10^-6;      %Length of Interdigitated Fingers (meters)
LG=3*10^-6;      %Gap Distance between interdigitated fingers (meters)
WT=3*10^-6;      %Width of Interdigitated Fingers (meters)
```

```matlab
T=2*10^-6;        %Thickness of Silicon Carbide Mechanical Layer (meters)
L0=10*10^-6;      %original length of axial length of finger gap
(meters)
ER=1.0;        %Relative Permittivity of Air (unit less)
EF=8.85419e-12;    %Permittivity of Free Space (Farads/meter)
NAFS=10;    %Axial Finger Sets quantity (unit less)
NIDFS=56;   %interdigitated finger set quantity (unit less) Use odd
number to make symmetric
YMSiC=340*10^3;  %Young's Modulus of Silicon Carbide (micronewtons per
square )
TSiCB=16*10^-6;    %Thickness of Flexible Backing SiC (meters)
LA=15*10^-6;   %Length of the anchor (meters)
LFace=178*10^-6;  %Length of applied load face (meters)
FA=1062;  %Applied Force (micronewtons per square micrometers)
Force=0:FA/2:FA; %Force Applied (micronewtons per square micrometers)

%Equations
    strain=Force/YMSiC;  %non micro strain
    eps=strain;  %conversion to micro strain
    DelL=eps*(LT+L0)      %Delta L relationship with strain
    CY=(ER*EF*(LT-(L0+DelL))*(T))/LG   %Yellow Region Capacitance
    CG=(ER*EF*(WT)*(T))*((L0+DelL).^-1)      %Green Region Capacitance
    CF=CY+CG        %Finger Set to region relationship
    CS=NAFS*(NIDFS*CF+CG) %Total Strain Sensor Capacitance

%Plot Mechanism
plot(eps,CS)     %Plot total strain sensor as a function of strain
title('Farads vs. Strain for the Mid Model')
xlabel('Strain')
ylabel('Farads')
```

Appendix B: Coventorware© Tools and Processes

Appendix B shows tools and processes used in this research for Coventorware©. L-Edit© is custom built MEMS software program developed by Tanner EDA© to layout, or draw, MEMS devices [19]. Coventorware© is a custom built MEMS software written by Coventor© for multiphysics finite element modeling and simulation [5].

B-1: Importing L-Edit© files into Coventorware©

Before the schematic can be simulated, the layout needs to be exported from L-Edit©, file type *.tdb or Tanner database file, to a file that can be imported into Coventorware©, *.gds file or graphic database system (GDS). After the file has been exported to a GDS file it cannot be imported until the manufacturing process is set into the process editor database of the Coventorware© project file. That process entered into the editor is shown in **Error! Reference source not found.**.

Using the process database in Figure 48, the L-Edit© layers need to be associated with the Coventorware© layers within the layout editor. The Coventorware© layers are named the same as the "Mask Names" from the process editor, for example the "Mech" mask name, for mechanical layer, is also the "Mech" layer. To export the L-Edit© layout file to GDS file format, the L-Edit© layers need to be associated to a GDSII layer. GDSII layer numbers are chosen for each of the L-Edit© layers, layer numbers are chosen at random. Those GDS layers are linked to the Coventorware© layers using the Coventorware© "layer browser". A screenshot of the "layer browser" is show in Figure 49.

Number	Step Name	Layer Name	Material Name	Thickness	Mask Name	Photoresist	Depth	Mask Offset	Sidewall Angle	Comments
0	Substrate	FlexSubstrate	SiCCrystaline	16	GND					
1	SiN Evaporation	SiNPassivatoin	SI3N4	0.2						The substrate is placed in a high vacuum
2	Conformal Shell	SiCTrace	PolySiC	0.2						
3	Straight Cut				Trace	+		0	0	remove sic trace pattern
4	Stack Material	Sacrifice	OXIDE	2						Sacrifitial Layer
5	Straight Cut				Anchor	-		0	0	remove SAC2
6	Conformal Shell Poly-SiC	Poly1	PolySiC	2						Poly Silicon Caribde Mechanical Layer
7	Straight Cut				Mech	+		0	0	remove poly-SiC
8	Delete		OXIDE							Release

Figure 48 Coventorware© Process Editor Database

Layer Name	Color	Fill	V	S	Layer Polarity on Mask	Mask Name	Dark/Light Mask Field	SAT/IGES	GDS	CIF/DXF	
GND	cyan	none	✓	✓	⦿+ ○-	GND	○D ⦿L	✓GND	✓L10D0	✓GND	🔍
Trace	green	dots1	✓	✓	⦿+ ○-	Trace	○D ⦿L	✓Trace	✓L12D0	✓Trace	🔍
Mech	red	solid	✓	✓	⦿+ ○-	Mech	○D ⦿L	✓Mech	✓L13D0	✓Mech	🔍
Anchor	yellow	solid	✓	✓	⦿+ ○-	Anchor	○D ⦿L	✓Anchor	✓L14D0	✓Anchor	🔍

Figure 49 Coventorware© Layer Browser for the Interdigitated Finger Layout

After the GDS file has been imported into Coventorware© it needs to be checked to verify the file imported fine. Figure 50 shows the layout editor as the imported layout file is verified.

Figure 50 Coventorware© Layout Editor with the Interdigitated Finger Set.

The layout is then opened in the mesh generator part of Coventorware©. When it is opened in the mesh generator software, a three dimensional model is created.

Bibliography

[1]   R. G. Azevedo, "A SiC MEMS Resonant Strain Sensor for Harsh Environment Applications," in IEEE Sensors Journal, Vol 7, No 4, April 2007.

[2]   R. G. Azevedo, J. Zhang; D. G. Jones, D. R. Myers, A. V. Jog, B. Jamshidi, M. B. J. Wijesundara, R. Maboudian, A. P. Pisano, "Silicon carbide coated MEMS strain sensor for harsh environment applications," Micro Electro Mechanical Systems, 2007. MEMS. IEEE 20th International Conference on , vol., no., pp.643-646, 21-25 Jan. 2007.

[3]   R. Cheung, "Introduction to Silicon Carbide (SiC) Microelectromechanical Systems (MEMS)," in Silicon Carbide Microelectromechancal Systems for Harsh Environments, London, England: Imperial College Press, 2006, ch. 1, pp. 3-4 and pp. 181.

[4]   R. Cheung, "Introduction to Silicon Carbide (SiC) Microelectromechanical Systems (MEMS)," in Silicon Carbide Microelectromechancal Systems for Harsh Environments, London, England: Imperial College Press, 2006, ch. 1, pp. 5-12.

[5]   (20, November 2011). CoventorWare Integrated Suite of Design Simulation Software Website. Available: http://www.coventor.com/products/coventorware/.

[6]   Y. Hezarjaribi, M. N. Hamidon, S. H. Keshmiri, A. R. Bahadorimehr, "Capacitive pressure sensors based on MEMS, operating in harsh environments," Semiconductor Electronics, 2008. ICSE 2008. IEEE International Conference on , vol., no., pp.184-187, 25-27 Nov. 2008.

[7]   Y. Hezarjaribi, "Capacitive Pressure Sensors Based on MEMS, Operating in Harsh Environments," in ICSE, Johor Bahru, Malaysia, 2009, pp. 184-187.

[8] K. Hoffman, "An Introduction to Measurements using Strain Gages". Darmstadt: Hottinger Baldwin Messtechnik GmbH, 1989. PP 52.

[9] R. C. Jaeger, "Thermal Oxidation of Silicon," in Introduction to Microelectronic Fabrication, 2nd ed. Upper Saddle River, New Jersey: Prentice-Hall Inc., 2002, ch. 3, pp. 43-54.

[10] R. C. Jaeger, "Processes for MicroElectroMechanical Systems: MEMS," in Introduction To Microelectronic Fabrication, 2nd ed. Upper Saddle River NJ: Prentice Hall, 2002, ch. 6 & 11, pp 129-138, pp. 271-273, and pp 279.

[11] L. Kretz, private communication, Jan-Aug, 2011.

[12] G. S. May and S. M. Sze, "Film Deposition," in Fundamentals of Semiconductor Fabrication. Wiley International Edition, 2004, ch. 8, sec. 8.3.2, pp. 89 and 160–162.

[13] M. Mehregany, C. A. Zorman, N. Rajan, C. H. Wu, "Silicon carbide MEMS for harsh environments," Proceedings of the IEEE , vol.86, no.8, pp.1594-1609, Aug 1998.

[14] W. M. Murray, W. R. Miller, "Stress-Strain Analysis and Stress-Strain Relations," in The Bonded Electrical Resistance Strain Gage. New York: Oxford University Press, 1992, ch. 2, pp. 42–89.

[15] W. M. Murray, W. R. Miller, "Fundamental Concepts for Strain Gages," in The Bonded Electrical Resistance Strain Gage. New York: Oxford University Press, 1992, ch. 1, pp. 3–41.

[16] C. R. Paul and S. A. Naser, "Electrostatic Fields: Capacitance," in Introduction to Electromagnetic Fields, 2nd ed. McGraw-Hill Book Company, New York: McGraw-Hill, Inc., 1987, ch. 3, pp. 127-134.

[17] (20, November 2011). Silicon Wafers for Semiconductor and optical applications Website. Available: http://www.siwafers.com/.

[18] W. C. Tang, "Electrostaic Comb Drive for Resonant Sensor and Actuator Applications," Ph.D. dissertation, Electrical Engineering and Computer Sciences, U. of California at Berkeley, Berkeley, CA, 1990, pp.12,14,26.   [18:12,14,26].

[19] (20, November 2011). Tanner EDA Software Tools – MEMS Design Website. Available: http://tannereda.com/mems.

[20] "U.S. Air Force Fact Sheet. AFRL/RB - Organization," USAF, Washington DC, 2011.

[21] D. M. Van Wie et. al., "The Hypersonic Environment: Required Operating Conditions and Design Challenges," in Journal of Materials Science., 2004, pp. 5915-5924.

[22] K. E. Wojciechowski, B. E. Boser, A. P. Pisano, "A MEMS resonant strain sensor operated in air," Micro Electro Mechanical Systems, 2004. 17th IEEE International Conference on. (MEMS) , vol., no., pp. 841- 845, 2004.

[23] C. A. Zorman, M. Mehregany, Edited by M. Gad-el-Hak "Materials for Microelectromechanical Systems," in MEMS, Design and Fabrication, 2nd ed. Boca Raton, CRC Press, 2006, ch. 2, pp. 2–9.

[24] C. A. Zorman, M. Mehregany, "Silicon carbide for MEMS and NEMS - an overview," Sensors, 2002. Proceedings of IEEE , vol.2, no., pp. 1109- 1114 vol.2, 2002.

1. REPORT DATE *(DD-MM-YYYY)*	2. REPORT TYPE	3. DATES COVERED *(From - To)*
22-03-2012	Master's Thesis	04-01-2009 - 22-03-2012

4. TITLE AND SUBTITLE	5a. CONTRACT NUMBER
Silicon Carbide Capacitive High Temperature MEMS Strain Transducer	Not Applicable
	5b. GRANT NUMBER
	Not Applicable
	5c. PROGRAM ELEMENT NUMBER
	Not Applicable

6. AUTHOR(S)	5d. PROJECT NUMBER
Weisenberger, Richard P, DR01	Not Applicable
	5e. TASK NUMBER
	Not Applicable
	5f. WORK UNIT NUMBER
	Not Applicable

7. PERFORMING ORGANIZATION NAME(S) AND ADDRESS(ES)	8. PERFORMING ORGANIZATION REPORT NUMBER
Air Force Institute of Technology Graduate School of Engineering and Management (AFIT/EN) 2950 Hobson Way Wright-Patterson AFB OH 45433-7765	AFIT/GE/ENG/12-43

9. SPONSORING/MONITORING AGENCY NAME(S) AND ADDRESS(ES)	10. SPONSOR/MONITOR'S ACRONYM(S)
Intentionally Left Blank	Not Applicable
	11. SPONSOR/MONITOR'S REPORT NUMBER(S)
	Not Applicable

12. DISTRIBUTION/AVAILABILITY STATEMENT

Distribution Statement A. Approved for public release; distribution is unlimited.

13. SUPPLEMENTARY NOTES

This material is declared a work of the U.S. Government and is not subject to copyright protection in the United States.

14. ABSTRACT

Air Force Research Lab Air Vehicles directorate performs research on hypersonic vehicles. To verify materials or designs of hypersonic vehicles, they have a need to measure strain at temperatures exceeding 700 C. Strain sensors have the ability to measure strain. Strain is the deformation of materials due to internal stresses in a material. Internal stresses occur when a material is subjected to a force. Traditional strain sensors use Piezoresistive effects to measure strain, which is temperature dependent and making them unusable at high temperatures. This paper discusses a novel strain sensing device, sensing capacitance instead of piezoresistance. The strain sensor is modeled mathematically and simulated using Coventorware©. The results are presented here, along with recommendations for future work.

15. SUBJECT TERMS

^MEMS, Micro-electro-mechanical Systems, Silicon Carbide, SiC, Poly-SiC, Strain Gage, Strain Sensor, Coventorware, Strain,

16. SECURITY CLASSIFICATION OF:			17. LIMITATION OF ABSTRACT	18. NUMBER OF PAGES	19a. NAME OF RESPONSIBLE PERSON
a. REPORT	b. ABSTRACT	c. THIS PAGE			Dr. Ronald Coutu
U	U	U	UU	101	**19b. TELEPHONE NUMBER** *(Include area code)* (937) 255-3636 x7230 ronald.coutu@afit.edu

Standard Form 298 (Rev. 8/98)
Prescribed by ANSI Std. Z39.18